Thermohaline Circulation Stability: a Box Model Study

by

Valerio Lucarini

Laurea Physics (1999)
University of Pisa, Italy

Diploma Physics (1999)
Scuola Normale Superiore, Italy

Submitted to the Department of Earth, Atmospheric, and Planetary Sciences
in partial fulfillment of the requirements for the degree of

Master of Science in Climate Physics and Chemistry

at the

MASSACHUSETTS INSTITUTE OF TECHNOLOGY

September 2003

Author .....
Department of Earth, Atmospheric, and Planetary Sciences
July 1st, 2003

Certified by .....
Peter H. Stone
Professor of Climate Dynamics
Thesis Supervisor

Accepted by .....
Maria T. Zuber
Head, Department of Earth, Atmospheric, and Planetary Sciences

Thermohaline Circulation Stability: a Box Model Study

by

Valerio Lucarini

Laurea Physics (1999)

University of Pisa, Italy

Diploma Physics (1999)

Scuola Normale Superiore, Italy

Submitted to the Department of Earth, Atmospheric, and Planetary Sciences
on July 1st, 2003, in partial fulfillment of the
requirements for the degree of
Master of Science in Climate Physics and Chemistry

Abstract

A thorough analysis of the stability of uncoupled and coupled versions of an inter-hemispheric 3-box model of Thermohaline Circulation (THC) is presented. The model consists of a northern high latitudes box, a tropical box, and a southern high latitudes box, which respectively can be thought as corresponding to the northern, tropical and southern Atlantic ocean. We study how the strength of THC changes when the system undergoes forcings that are analogous to those of global warming conditions. In each class of experiments, we determine, using suitably defined metrics, the boundary dividing the set of forcing scenarios that lead the system to equilibria characterized by a THC pattern similar to the present one, from those that drive the system to equilibria where the THC is reversed.

In the case of the uncoupled model, we apply to the equilibrium state perturbations to the moisture and heat fluxes into the three boxes. High rates of increase in the moisture flux into the northern high-latitude box lead to a THC breakdown at smaller total final increases in the moisture flux than low rates, while the presence of moisture flux increases into the southern high-latitude box strongly inhibit the breakdown and can prevent it, in the case of slow rates in the Northern Hemisphere. Similarly, a fast heat flux increases in the North Hemisphere destabilize the system more effectively than slow ones, and again the enhancement of the heat fluxes in the Southern Hemisphere tend to drive the system towards stability. In all cases analyzed slow forcings, if sufficiently weak in the Southern Hemisphere, lead to the reversal of the THC.

In the coupled model a direct representation of the radiative forcing is possible, since the main atmospheric physical processes responsible for freshwater and heat

fluxes are formulated separately. Although only weakly asymmetric or symmetric radiative forcings are representative of physically reasonable conditions, we consider general asymmetric forcings, in order to get a more complete picture of the mathematical properties of the system. We also consider different choices for the atmospheric transport parametrizations and for the ratio between the high latitude to tropical radiative forcing, and analyze the senstivity of our results to changes in these parameters. We generally find that fast forcings are more effective than slow forcings in disrupting the present THC patterns, forcings that are stronger in the northern box are also more effective in destabilizing the system, and that very slow forcings do not destabilize the system whatever their asymmetry, unless the radiative forcings are very asymmetric and the atmospheric transport is a relatively weak function of the meridional temperature gradient. The changes in the strength of the THC are primarily forced by changes in the latent heat transports, because of their sensitivity to temperature that arises from the Clausius-Clapeyron relation.

Thesis Supervisor: Peter H. Stone
Title: Professor of Climate Dynamics

Acknowledgments

I thank Peter Stone for being both a great advisor and mentor, for having always been extremely supportive and flexible, and for having provided excellent intellectual stimulations.

I wish to emphasize my gratitude to the Department of Earth, Atmospheric, and Planetary Sciences and the Joint Program on the Science and Policy of the Global Change for opening new worlds in my studies.

I also wish to thank Gary Russell, David Rind, and Gavin Schmidt of GISS, NASA, for their help and stimulations during my summer residency at GISS in 2001; Myles Allen and Lenny Smith for providing intellectual stimulations; Stefan Rahmstorf and Andrey Ganopolski for the permission to reproduce some figures; Vincenzo Artale and Sandro Calmanti for suggestions and help; Lodovica Illari for technical and emotional support and for being a great lecturer; Paola Malanotte for continous understanding and for being an example; Franco Bassani for support and counseling; Kai Peiponen for his *science as friendship* style; Nicholas Ashford for his intellectual honesty; Jeff Scott for several comments; Fabio Dalan and Diego Puppin, my tender Italian peers in New England; Peter Vickers, for showing me how brave the new world is; Paolo Marchi, because he does not give up; Francesco Gullá and Silvia Veroli, no need to say anything; and all the friends of the Forum Energia in Florence, for giving me so much.

I have to thank Cambridge and Boston for the unforgettable, wonderful, chilly winds on the Harvard Bridge and for the snow in winter, and for the deep blue sky in fall.

Hugs, hugs and kisses to my parents for their presence. A huge kiss to my grandfather, who sadly is not with us anymore, and to my grandmother.

Infinite love and thanks to Giovanna: nothing vaguely compares to you.

This dissertation is dedicated to the everlasting memory of Matteo: it is two years, it seems yesterday; even while writing this very sentence, tears fall once more.

Biographical Notes

Essential information

Valerio Lucarini was born in Ancona, Italy, on August 11th 1976. He is an Italian citizen. He presently lives in via Panicale 10, 50123 Florence, Italy. Tel: +39-3488814008. Email: lucarini@mit.edu.

Education

Valerio Lucarini graduated in Physics at the University of Pisa, Italy, with 110/110 cum Laude in 1999, and in the same year he was granted the Diploma of Physics by the Scuola Normale Superiore, Italy, with 70/70 cum Laude. In September 2000 he was admitted as graduate student at the Department of Earth, Atmospheric and Planetary Sciences, MIT.

Honors and Awards

Full fellowship by the Scuola Normale Superiore, Italy, 1995-1999.
Full fellowship by the École Normale Superiéure, France, December 1997.
Full fellowship by the Masachusetts Institute of Technology, 2000-2002.
Charney prize by the Department of Earth, Atmospheric and Planetary Sciences of MIT, 2000.
Somaini prize by the Italian Physical Society (SIF), 2000.
Global Change Scholarship by the American Meteorological Society, 2001

Work experiences

Valerio Lucarini worked for three months in 1999 as system administrator for a Microsoft Windows cluster of the Scuola Normale Superiore. He visited the Goddard

Institute for Space Studies (GISS) in New York, NY, during the Summer 2001 and interacted with the Atmosphere Ocean Model group (AOM). Valerio Lucarini is currently volunteering as teaching assistant in the didactic program of the University of Florence at the Prato National Prison.

Selected Publications

- La scienza del clima (in Italian), V. Lucarini, Equilibri 3, 307-319 (2001);
- Towards a definition of Climate Science, V. Lucarini, International Journal of Environment and Pollution 18 (5), 413-422 (2002);
- Comparison of mean climate trends in the Northern Hemisphere between NCEP and two GISS Atmosphere-Ocean model forced runs - published by the Journal of Geophysical Research- Atmospheres 107, DOI:10.1029/2001JD001247 (2002).

Submitted papers

- Thermohaline Circulation Stability: a box model study: Part I: uncoupled model, submitted to the Journal of Climate;
- Thermohaline Circulation Stability: a box model study: Part II: coupled atmosphere-ocean model, submitted to the Journal of Climate;
- Reallocation of Power and Sustainable Development, submitted to the International Journal of Sustainable Development.

Contents

List of Figures

List of Tables

Chapter 1

Introduction

1.1 The Thermohaline Circulation

1.1.1 Few remarks on the energetics of the Thermohaline Circulation

Following the classical picture of Sandström's, the ocean circulation can be divided, albeit somewhat ambiguously, in wind-driven circulation, which is directly induced by the mechanical action of the wind and essentially regards the surface waters, and in thermohaline (THC) circulation, which is characterized by relatively robust gradients in the buoyancy of the water masses [Weaver and Hughes 1992, Weaver et al. 1999, Rahmstorf 2000, Rahmstorf 2002, Stocker et al. 2001]; the THC dominates the large scale picture of the global ocean circulation and is especially relevant for the indemediate-to-deep water.

Sandström theorem shows that buoyancy forcings can generate steady currents only if the negative density perturbations occur at greater depth than the positive density perturbations. In the real ocean system the buoyancy forcings are pertubations to temperature and salinity -thus thermohaline perturbations-, which, apart from the rather small geothermal contribution, are caused by the surface heat and freshwater fluxes. Therefore buoyancy forcing alone cannot be the driving mechanism of the THC. The deep *buoyancy source* that causes the circulation is obtained as effect of efficient turbolent mixing, powered by wind and tides, which therefore provide the energetics of the THC [Wunsch and Ferrari 2004]. A reasonable global picture is that the large scale motion of water masses is driven by the surface heat and freshwater fluxes and by the turbolent mixing of heat and salt occurring in the interior of the ocean [Rahmstorf 2003].

1.1.2 Phenomenology of the Thermohaline Circulation

In the northern Atlantic ocean, in the Greenland-Iceland-Norwegian Seas, dense water masses are formed in the surface, they downwell to the bottom of the ocean and move southward by deep western boundary currents to the southern Atlantic, from where they depart to fill the bottom of the Indian and Pacific Oceans; the water masses then upwell and the return flow closes up with the northern advection by the northern Atlantic branch of the Gulf Stream of the very warm and saline water from the tropics. The strong heat and freshwater exchange of the anoumalous water with cold polar air

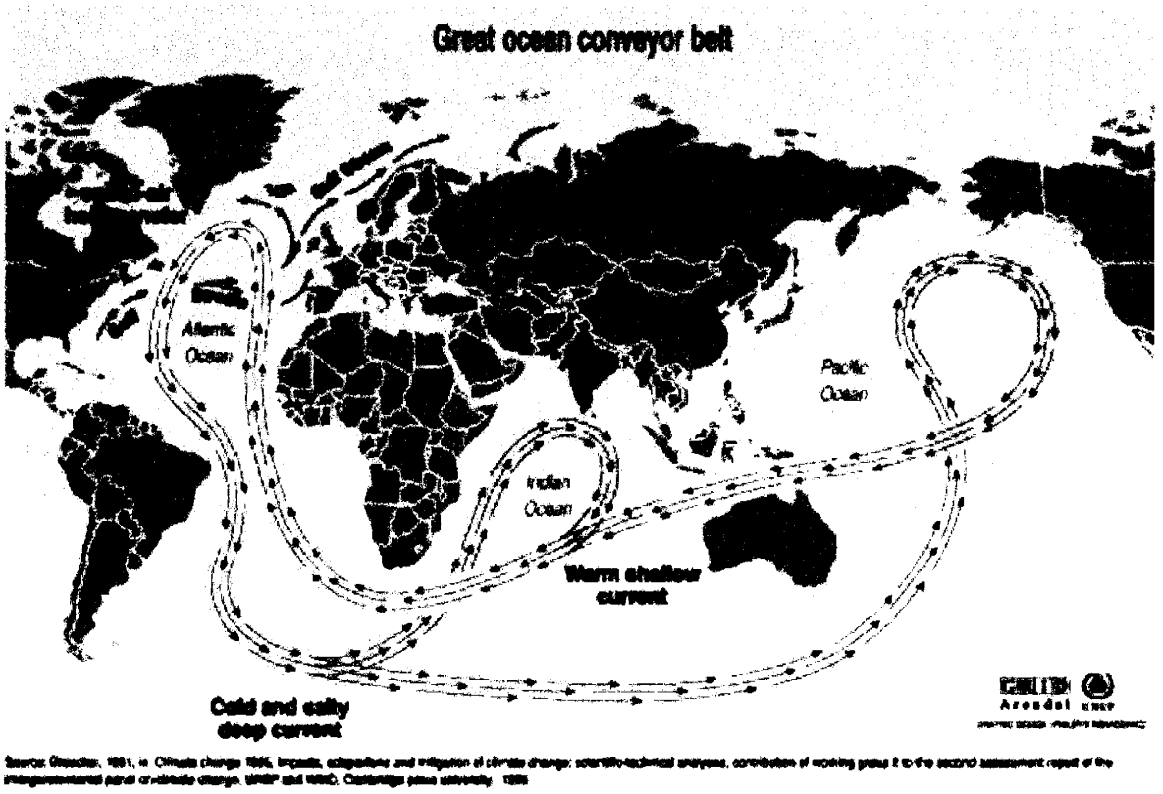

Figure 1-1: Simplified picture of the Thermohaline Circulation pattern - from the United Nations Environment Programme-GRID Arendal (Norway) web site http://www.grida.no/climate/

masses allow the formation of the North Atlantic Deep Water (NADW). In figure 1-1 we report the simplified *conveyor belt* [Broecker 1991] picture of the large scale ocean circulation, whose time scale is of the order of 1000 years. The limitations of this powerful and synthetic image have nevertheless been later underlined: more complex structures emerge from observations and modelling [Macdonald and Wunsch 1996].

The THC plays a crucial role in determining the main features of the North Atlantic climate [Levitus 1982] (see figure 1-2), since the advection of warm water prevents the formation of sea ice up to very high latitudes even during winter. Past studies suggested that the THC-driven heat exchange between relatively warm water and cold air was the main mechanism providing Europe with a much milder climate than other areas on the globe located at similar latitudes [Broecker 1994, Rahmstorf and Ganopolski 1999, Stocker 2000, Stocker et al. 2001]; very recent studies nevetheless suggest that the relatively temperate European climate is mainly due to the northward atmospheric heat advection caused by the transient eddies of the

storm system [Seager et al. 2002]. Since the world climate is affected by the presented pattern of the large scale ocean circulation, a change in the intensity or, *a fortiori*, of the pattern of the THC may have global effects, even if it is expected that the temperatures of the northern Atlantic regions would be the most sensitive climatic variable in case of a shut off of the THC (see figure 1-3) [Broecker 1997, Manabe and Stouffer 1999b, Cubasch et al. 2001, Rahmstorf 2002]. Anyway, on longer time scales, the global climatic influence of the THC can be appreciated by ackowledging its fundamental role in the redistribution of nutrients at global scale, its strong influence on the gaseous and especially CO2 uptake of the ocean, and its influence on the planetary albedo due to the control of the extent of the sea ice in the northern Atlantic. On the other hand, the THC is sensitive to changes in the climate since the

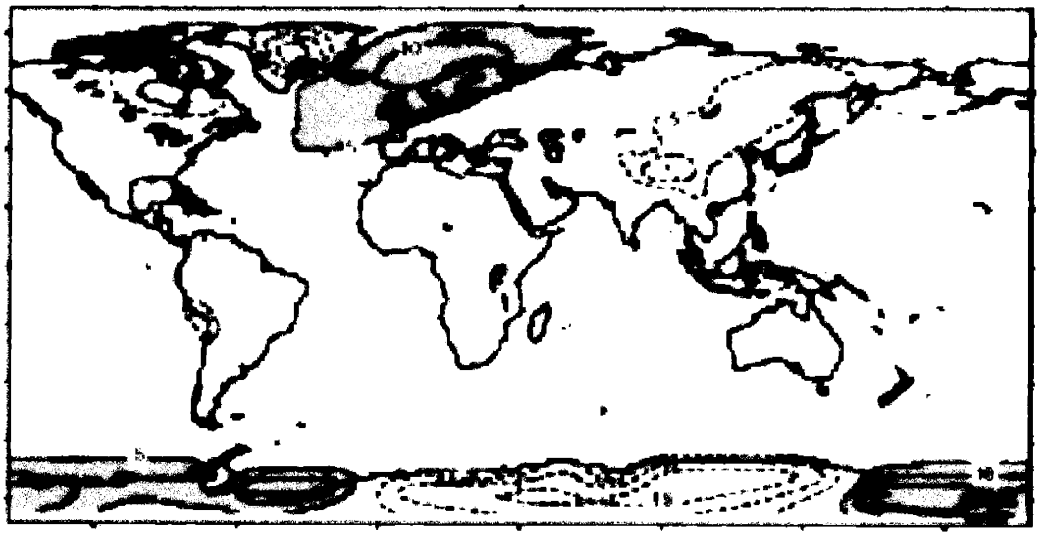

Figure 1-2: Climatological zonal temperature anomalies from NCAR data; abscissae in latitudinal and ordinates in longitudinal degrees; data are in $^{\circ}C$ - reproduced with permission from [Rahmstorf and Ganopolski 1999]

NADW formation is especially sensitive to variations in air temperature and in precipitations in the Atlantic basin [Rahmstorf and Willebrand 1995, Rahmstorf 1996]. We then understand that the Atlantic basin plays a particularly important role in the world ocean circulation, and the value of the meridional overturning circulation (see figure 1-4) in the North Atlantic is the most relevant measure of the intensity of the THC. In our work we will then concentrate on the dynamics of the circulation of the Atlantic basin.

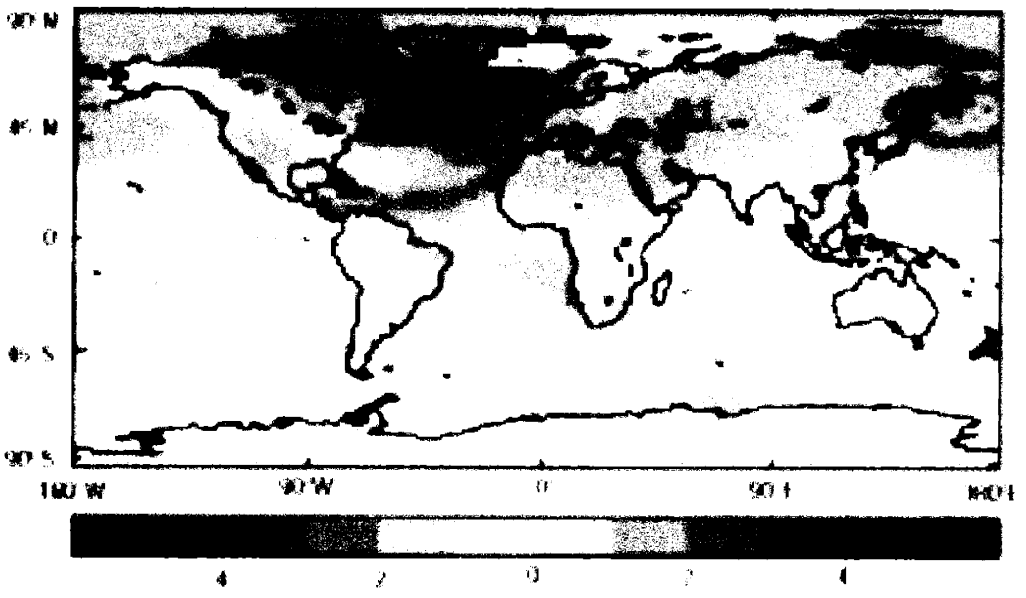

Figure 1-3: Temperature Changes for an abrupt shut off of the Thermohaline Circulation; data are in $^{\circ}C$ - reproduced with permission from [Rahmstorf 2002]

1.2 Stability of the Thermohaline Circulation

In the last years the scientific community has paid a great deal of attention to the study of the possibility of nonlinear changes in the climate system. The most interesting intrinsic features of these transitions are that they may have very limited predictability, may have large scale effects resulting from local forcings, may be irreversible, may manifest themselves as *surprises*, i.e., take place without being announced by comparatively large precusors. These stiff properties, which distinctively mark *complexity*, allow us to understand why we still have a relatively poor representation of these processes even in the best available climate models: a more complete understanding of the main feedback mechanisms is still needed. Among those nonlinear processes we can point out large scale land-use changes, Antarctica ice-sheet collapse, permafrost thawing,and the collapse of the THC.

Since the seminal paper [Broecker et al. 1985], the issue of determing if the world -and Atlantic in particular- ocean circulation has more than one stable states and can undergo hysteresis cycles has attracted a very large interest [Ganopolski and Rahmstorf 2001b] , especially after that several paleoclimatic data sets have indicated that dramatic changes in the patterns or collapses of the THC coincide with large variations in climate [Boyle and Keigwin 1987, Keigwin et al. 1994, Keigwin and Boyle 2000].

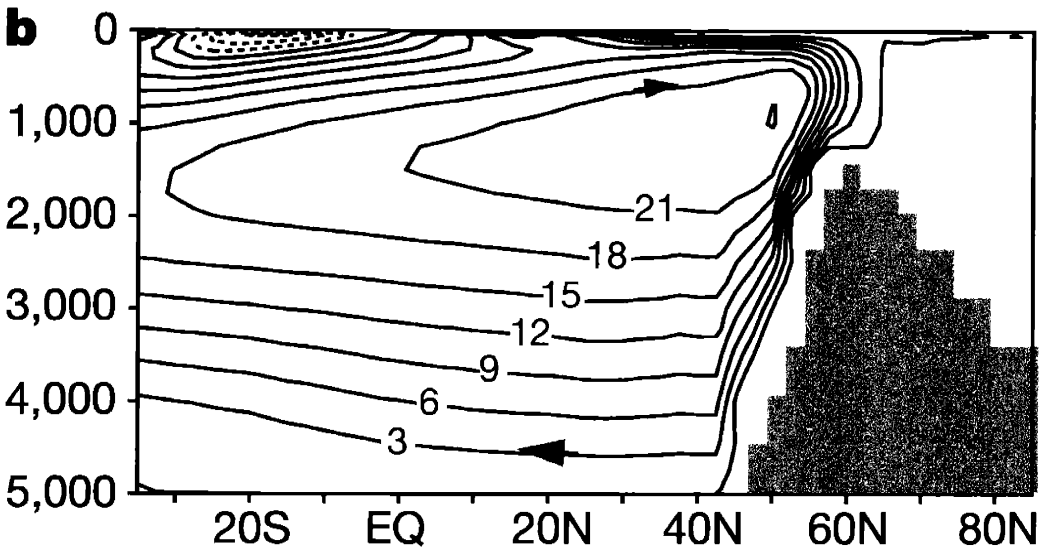

Figure 1-4: Modelled streamfuction of the North Atlantic; abscissae in longitudinal degrees and ordinates in meters; data in Sv - reproduced with permission from [Ganopolski and Rahmstorf 2001a]

Probably the most outstanding features of these climate changes is their abruptness and the large scale geographic syncronization, which involves regions far beyond the northern Atlantic area [Blunier et al. 1997, Vidal et al. 1999]. The signature of the involment of THC in these climatic swings can be found in the recently discovered covariance between temperature changes at various depths [Adkins et al. 1998]. In particular three main modes (see figure 1-5) of THC have been identified [Rahmstorf 2002] in the paleoclimatic reconstructions: *interglacial* mode (like the present), *glacial* (ice age-like) mode, and *Heinrich* (typical of Heinrich cold events [Vidal et al. 1999]) *off* mode. In the latter case the Antarctic Bottom Water (AABW), which is the densest water in the planet, formed in the under the iceshelves of Antarctica, is advected all the way to the North Atlantic, thus where it upwells, so that the circulation is substantially reversed with respect to the present state. Various GCM experiments have confirmed that multiple equilibria of the THC are possible [Bryan 1986, Manabe and Stouffer 1988, Stouffer et al. 1991, Stocker and Wright 1991, Manabe and Stouffer 1999a, Marotzke and Willebrandt 1991, Hughes and Weaver 1994]. Along these lines one of the main issues in the study of the climate change is the fate of the THC in the context of global warming [Weaver and Hughes 1992, Manabe and Stouffer 1993, Stocker and Schmittner 1997, Rahmstorf 1997, Rahmstorf 2002, Wang et al. 1999a, Wang et al. 1999b]. Following the seminal work by Manabe and Stouffer (see figure 1-6), most GCMs have shown that greenhouse gases (GHGs) induced radiative

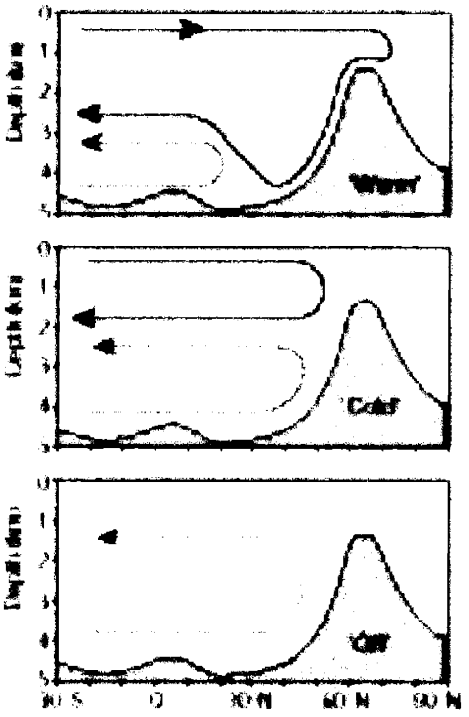

Figure 1-5: Three main modes of Thermohaline Circulation, from top to bottom: interglacial ("warm"), glacial ("cold") and Heinrich ("off") modes; purple line NADW, blue line AABW - reproduced with permission from [Rahmstorf 2002]

forcing could cause a weakening of the THC by the inhibition of the sinking of the water in the northern Atlantic [Cubasch et al. 2001], as can be seen in figure 1-7. The weakening of the THC in a global warming scenario could limit the regional warming in the eastern side of the North Atlantic [Rahmstorf 1997, Rahmstorf 1999a, Rahmstorf 1999b, Rahmstorf 2000]. Large increases of the moisture flux and/or of the sea surface temperature in the downwelling regions are the driving mechanisms of such a process. While earlier studies proposed that fast CO_2 increases could eventually cause the shutdown of the THC, some more recent studies seem to suggest that the THC can eventually recover also from very low values [Stouffer and Manabe 2003]. We underline that in the global warming simulation run with the *ECHAM-4* model (brown line in figure 1-7) the THC remained almost constant since the destabilizing mechanisms have been offset by the increase of the salinity advected in the downwelling region due to net freshwater export from the whole North Atlantic [Latif et al. 2000].

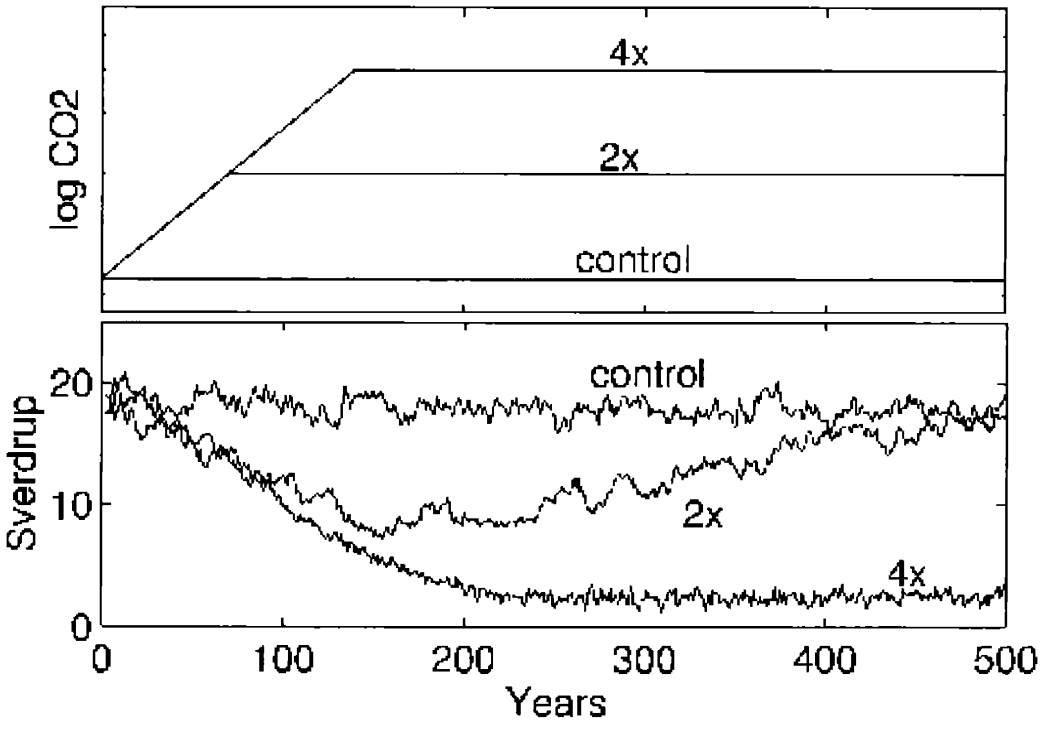

Figure 1-6: Simulations of Thermohaline Circulation change under global warming scenarios - adapted from [Manabe and Stouffer 1993]

1.3 Box Models

Box models have historically played a major role in the understanding of the fundamental dynamics of the THC [Weaver and Hughes 1992]. The Stommel two-box oceanic model [Stommel 1961] built the first conceptual bridge between the THC strength and density gradients. The oceanic model proposed by Rooth [Rooth 1982] introduced the idea that the THC was described by density difference between the high latitudes basins of the northern and southern hemispheres, thus implying that the THC is an inter-hemispheric phenomenon. Both the Stommel and Rooth models allow two stable equilibria, one -the warm mode- characterized by downwelling of water in the North Atlantic, which resembles the present oceanic circulation, and the other - the cold mode - characterized by upwelling of water in the North Atlantic. Perturbations to the driving parameters of the system, i.e. freshwater and heat fluxes in the oceanic boxes, can cause transitions between the two regimes. We underline that since box models are characterized by perfect mixing inside each box, they have the intrinsic limitation of not assessing properly the energetic problem previously mentioned at the beginning of the chapter.

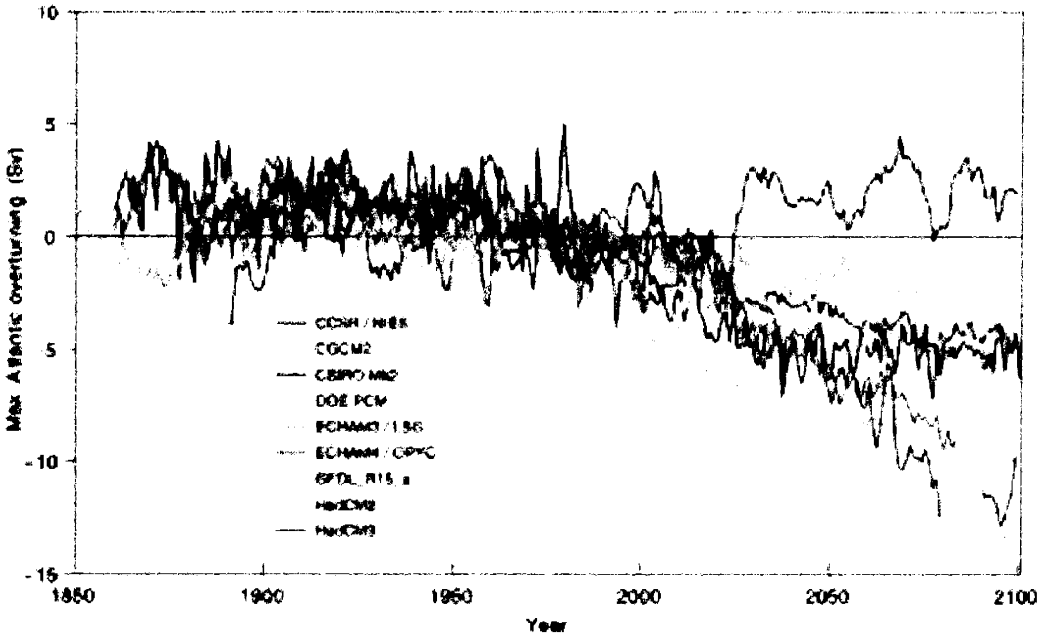

Figure 1-7: Simulated merdional overturning change of the THC in a range of global warming scenarios computed by different climate research centres; Shown is the annual mean relative to the mean of the years (1961 to 1990); abscissae in years and ordinates in Sv - from [Cubasch et al. 2001]

Analysis of GCM data have also indicated that the THC is definitely not an Atlantic basin hemispheric phenomenon [Stocker et al. 2001, Stocker 2002], and in some cases it has been found that the THC strength is approximatively proportional to the density difference between the northern and southern Atlantic [Hughes and Weaver 1994, Rahmstorf 1996, Klinger and Marotzke 1999, Wang et al. 1999a], thus supporting Rooth's approach. While hemispheric box models like Stommel's have been extensively studied [Weaver and Hughes 1992, Nakamura et al. 1994, Marotzke 1996, Krasovskiy and Stone 1998, Tziperman and Gildor 2002], and the stability of their THC has been assessed in the context of various levels of complexity in the representation of the coupling between the ocean and the atmosphere, the literature on inter-hemispheric box models is far less abundant [Rahmstorf 1996, Scott et al. 1999, Stone and Krasovskiy 1999, Titz et al. 2002a, Titz et al. 2002b], and few studies have included the effect of coupling an inter-hemispheric model of the ocean to the atmosphere [Scott et al. 1999, Stone and Krasovskiy 1999, Tziperman and Gildor 2002].

1.4 Outline of our study

In this study we perform an analysis of the stability of the present pattern of the THC against changes to the heat and freshwater atmospheric fluxes using three versions of the interhemispheric 3-box oceanic model first presented by Rooth [Rooth 1982]; these versions greatly differ in their representation of the coupling between the ocean and the atmosphere. The first model has no real explicit coupling between the ocean and the atmosphere: the atmospheric freshwater fluxes are prescribed and the atmospheric heat fluxes relax the oceanic temperatures towards prescribed values. The second model differs from the first since there is no oceanic temperature relaxation: the heat fluxes are also prescribed. The third model has explicit coupling between the ocean and the atmosphere: the atmospheric freshwater and heat fluxes are expressed as functions of the oceanic temperatures. In particular this model presents the very relevant feature of including the Clausius-Clapeyron effect on moisture and latent heat fluxes in a parameter study of how global warming affects the THC. In the case of GCMs, where obviously the Clausius-Clapeyron relations are included in the physical description of the atmosphere, parameter studies cannot be performed, while this strongly nonlinear effect has been left out of several interhemispheric box models and Earth Models of Intermediate Complexity (EMICS) [Stone and Krasovskiy 1999, Scott et al. 1999, Wiebe and Weaver 1999, Petoukhov et al. 2000]. We explicitly analyze, to the extent that the simplicity of the model allows, what is the role of the spatial patterns *and* of the rates of increase of the forcings to the driving parameters and characterize the response of the system. We determine, using suitably defined metrics, which are the thresholds beyond which we have destabilization of the warm mode of the THC. We underline that our treatment goes beyond quasi-static analysis since the effect of the rate of forcing is explicitly addressed, so that we analyze how the effects on the system of slow [Wang et al. 1999a] and rapid [Wiebe and Weaver 1999] changes join on; in particular in the limit of very slow changes, our results coincide with those that could be obtained with the analysis of the bifurcations of the system [Stone and Krasovskiy 1999, Scott et al. 1999, Titz et al. 2002a, Titz et al. 2002b]. We underline that since we consider only poleward freshwater fluxes, our study differs from Rahmstorf's [Rahmstorf 1996]. Only relatively few studies have explicitly addressed how the spatial [Rahmstorf 1995, Rahmstorf 1996, Rahmstorf 1997] or temporal [Stocker and Schmittner 1997, Schmittner and Stocker 1999] patterns of forcing determine the response and allow the investigation of the stability properties

of the system in the context of more complex models, but obvious limitations due to computing time did not allow an extensive exploration of the parameter space of the forcings applied, nor allowed a parametric study of the influence of both spatial *and* temporal patterns.

1.5 Model description

The three-box model consists of a northern high latitude box (box 1), a tropical box (box 2), and a southern high latitude box (box 3). The volume of the two high latitudes boxes is the same, and is $1/V$ times the volume of the tropical box. We choose $V = 2$, so that box 1, box 2 and box 3 respectively can be thought as describing the portions of an ocean like the Atlantic north of $30°N$, between $30°N$ and $30°S$, and south of $30°S$. At the eastern and western boundaries of the oceanic boxes there is land; our oceanic system spans 60° in longitude, so that it covers $\epsilon = 1/6$ of the total surface of the planet. The boxes are 5000 m deep, so that the total mass $M_{i=1,3} = M$ of the water contained in each of the high-latitude boxes is $\approx 1.1 \cdot 10^{20}\ Kg$, while $M_2 = V \cdot M_{i=1,3} = 2 \cdot M$. The tropical box is connected to both high latitude boxes; moreover the two high latitude boxes are connected by a deep current passage (which bypasses the tropical box) containing a negligible mass. The three boxes are assumed to be well mixed, so that the *polar halocline*

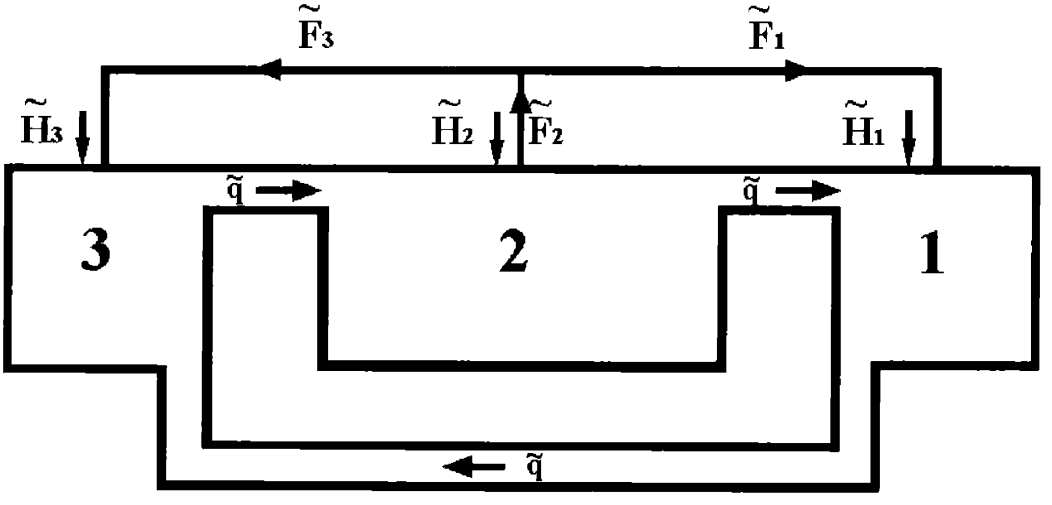

Figure 1-8: Schematic picture of the interhemispheric box model

disaster [Bryan 1986, Zhang et al. 1993] is automatically excluded from the range of phenomena that can be described by this model. The physical state of the box i

is described by its temperature T_i and its salinity S_i; the box i receives from the atmosphere the net flux of heat $\tilde{H}_i$ and the net flux of freshwater $\tilde{F}_i$; the freshwater fluxes $\tilde{F}_i$ globally sum up to 0, since the freshwater is a globally conserved quantity. The box i is subjected to the oceanic advection of heat and salt from the upstream box through the THC, whose strength is $\tilde{q}$. In figure 1-8 we present a scheme of our system in the northern sinking pattern: note that the arrows representative of the freshwater fluxes are arranged in such a way that the relative conservation law is automatically included in the graph. The dynamics of the system is described by the tendency equations for the heat and the salinity of each box. We divide the three heat tendency equations by $c_p \cdot M_i$, where c_p is the constant pressure specific heat of water per unit of mass, and in the salinity tendency equations we neglect the contribution of the freshwater fluxes in the mass balance, so that virtual salinity fluxes and freshwater fluxes are equivalent [Marotzke 1996, Rahmstorf 1996, Scott et al. 1999]. We obtain the following final form for the temperature and salinity tendency equations for the three boxes [Scott et al. 1999]:

$$\dot{T}_1 = \begin{cases} q(T_2 - T_1) + H_1, & q \geq 0 \\ q(T_1 - T_3) + H_1, & q < 0 \end{cases} \tag{1.1}$$

$$\dot{T}_2 = \begin{cases} \frac{q}{V}(T_3 - T_2) + H_2, & q \geq 0 \\ \frac{q}{V}(T_2 - T_1) + H_2, & q < 0 \end{cases} \tag{1.2}$$

$$\dot{T}_3 = \begin{cases} q(T_1 - T_3) + H_3, & q \geq 0 \\ q(T_3 - T_2) + H_3, & q < 0 \end{cases} \tag{1.3}$$

$$\dot{S}_1 = \begin{cases} q(S_2 - S_1) - F_1, & q \geq 0 \\ q(S_1 - S_3) - F_1, & q < 0 \end{cases} \tag{1.4}$$

$$\dot{S}_2 = \begin{cases} \frac{q}{V}(S_3 - S_2) - F_2, & q \geq 0 \\ \frac{q}{V}(S_2 - S_1) - F_2, & q < 0 \end{cases} \tag{1.5}$$

$$\dot{S}_3 = \begin{cases} q(S_1 - S_3) - F_3, & q \geq 0 \\ q(S_3 - S_2) - F_3, & q < 0 \end{cases} \tag{1.6}$$

where $q = \rho_0 \cdot \tilde{q}/M$, $H_i = \tilde{H}_i/(c_p \cdot M)$, and $F_i = \rho_0 \cdot S_0 \cdot \tilde{F}_i/M$. We impose that the average salinity is a conserved quantity; this means that $\dot{S}_1 + V\dot{S}_2 + \dot{S}_3$=0, which implies that:

$$F_2 = -\frac{1}{V}(F_1 + F_3). \tag{1.7}$$

This conservation law holds at every time, and so rules out the possibility of including in our study the effects of the melting of continental ice sheets.

On the other hand we do not impose any strict conservation law for the transient behavior of the global heat budget of the ocean, since we essentially want to include the effects of radiative imbalances. We note that the system can (asymptotically) reach an equilibrium only if its feedbacks can drive it towards a state in which the following equation holds:

$$H_2 = -\frac{1}{V}(H_1 + H_3). \tag{1.8}$$

The strength of the specific THC, along the lines of the Stommel model [Stommel 1961], is parametrized as proportional to the difference between the density of the water contained in the box 1 and the density of the water contained in the box 3. Given that the water density can approximately be expressed as:

$$\rho(T, S) \approx \rho_0(1 - \alpha T + \beta S); \tag{1.9}$$

where α and β are respectively the thermal and haline expansion coefficients, set respectively to $1.5 \cdot 10^{-4}\ ^\circ C^{-1}$ and $8 \cdot 10^{-4}\ psu^{-1}$, and ρ_0 is a standard reference density, we obtain for the normalized THC strength q the following relation:

$$q = \frac{k}{\rho_0}(\rho_1 - \rho_3) = k(\alpha(T_3 - T_1) + \beta(S_1 - S_3)), \tag{1.10}$$

where k is the hydraulic constant, whose value is such that we obtain a reasonable value of the THC strength. The northern (southern) sinking state of the circulation is therefore characterized by $q > (<)0$. Considering the case $q > 0$, we obtain a diagnostic relation for steady state q by setting to 0 equations 1.3 and 1.6, and using equation 1.9:

$$q_{eq} = (k(\alpha((H_3)_{eq} + \beta(F_3)_{eq})))^{1/2}; \tag{1.11}$$

in the case $q < 0$, a diagnostic relation for the steady state q can be obtained using the same procedure as above but setting to zero equations 1.1 and 1.4:

$$q_{eq} = -(k((\alpha(H_1)_{eq} + \beta(F_1)_{eq}))^{1/2}. \tag{1.12}$$

We conclude that the *equilibrium* value of the THC strength is determined by the equilibrium values of the heat and freshwater fluxes of the box where we have upwelling of water. These results generalize the expressions given by Rahmstorf [Rahmstorf 1996].

The transient evolution of q is determined by its tendency equation:

$$\begin{aligned}\dot{q} = &- q^2 + kq(\alpha(T_1 - T_2) - \beta(S_1 - S_2))+ \\ &+ k(\alpha(H_3 - H_1) + \beta(F_3 - F_1)), \quad q \geq 0,\end{aligned} \tag{1.13}$$

$$\begin{aligned}\dot{q} = &q^2 + kq(\alpha(T_3 - T_2) - \beta(S_3 - S_2))+ \\ &+ k(\alpha(H_1 - H_3) + \beta(F_1 - F_3)), \quad q < 0.\end{aligned} \tag{1.14}$$

We observe that the difference between the forcings applied to the freshwater and heat fluxes into the two boxes 1 and 3 directly effect the evolution of q; the presence of terms involving the gradient of temperature and salinity between box 2 and box 1 (box 3) if $q > 0$ ($q < 0$) breaks the symmetry of the role played by the two high latitude boxes. In our experiments we perturb an initial equilibrium state -which is the same for all the experiments in all of the three versions of the model analyzed- by changing at various rates the parameters controlling the fluxes H_i and/or F_i and observe under which conditions we obtain a reversal of the THC. The reversal of the THC causes a sudden cooling and freshening in the box 1 and a sudden warming and increase of the salinity in the box 3, because the former loses and the latter receives the advection of the tropical warm and salty water.

Chapter 2

Uncoupled Model with Mixed Boundary Conditions

2.1 Description of the Rooth model

The first version of the model is the Rooth model in its original formulation [Rooth 1982]. For a more detailed description of the model see also the reference [Scott et al. 1999]. In this model the atmosphere has a negligible heat capacity and water content compared to the ocean, and it only transports heat and moisture; the land has also negligible heat capacity, so that all the heat fluxes end up in the oceanic fraction of the total planetary surface. The heat flux into the box i is described by a newtonian relaxation law of the form $H_i = \lambda_i(\tau_i - T_i)$ where the parameter τ_i is the target temperature [Bretherton 1982], which represents a climatologically reasonable value towards which the box temperature is relaxed, and the parameter λ_i quantifies the efficacy of the relaxation. We then make a choice of the values of these parameters and integrate from reasonable initial conditions in order to define a northern sinking equilibrium state that is the baseline for all the rest of the study. Along the lines of the reference [Scott et al. 1999] and following the parametrization introduced in reference [Marotzke 1996], we choose $\tau_1 = \tau_3 = 0°C$ and $\tau_2 = 30°\ C$, and select $\lambda_1 = \lambda_2 = \lambda_3 = \lambda = 1.29 \cdot 10^{-9}\ s^{-1}$, which mimics the combined effect of radiative heat transfer and of a meridional heat transport parameterized as linear with the meridional temperature gradient [Marotzke and Stone 1995, Marotzke 1996, Scott et al. 1999]. In physical terms, λ corresponds to a restoring coefficient of $\approx 4.3\ Wm^{-2}\ °C^{-1}$ affecting the whole planetary surface, which translates into an effective $\tilde{\lambda} \approx 1/\epsilon \cdot 4.3\ Wm^{-2}\ °C^{-1} = 25.8\ Wm^{-2}\ °C^{-1}$ relative to the oceanic surface fraction only. Using equations 1.1, 1.2, and 1.3, we can obtain the following tendency equation for the globally averaged temperature $T_M = (T_1 + VT_2 + T_3)/(2 + V)$:

$$\dot{T}_M = \lambda(\tau_M - T_M) \tag{2.1}$$

where τ_M is the average target temperature; the average temperature relaxes towards its target value in about 25 y, which is very close to the value considered in [Titz et al. 2002a]; we observe that in the case of an ocean represented with vertical resolution, our heat flux parametrization corresponds to a restoring time of ≈ 3 months for a 50 m deep surface level [Marotzke and Stone 1995].

The virtual salinity fluxes F_i are not functions of any of the state variables of the system, and are given parameters. We choose $F_1 = 13.5 \cdot 10^{-11}\ psu\ s^{-1}$ and $F_3 = 9 \cdot 10^{-11}\ psu\ s^{-1}$, which respectively correspond to net atmospheric freshwater fluxes of $\approx 0.40\ Sv$ into the box 1 and of $\approx 0.27\ Sv$ into the box 3. The ratio-

nale for the chosen asymmetry in the freshwater fluxes lies in the analysis of the hydrology of the two hemispheres done in reference [Baumgartner and Reichel 1975]. Choosing $k = 1.5 \cdot 10^{-6}\ s^{-1}$, at equilibrium we have $q \approx 1.47 \cdot 10^{-10}\ s^{-1}$ [Scott et al. 1999], which corresponds to an oceanic flushing time scale of $\approx 300\ y$; in physical terms the previous value for q describes a THC in the northern sinking pattern with a strength of $\approx 15.5\ Sv$: this value agrees reasonably well with estimates coming from observations [Roemmich and Wunsch 1985, Macdonald and Wunsch 1996]. The equilibrium temperature of box 1 is larger than the equilibrium temperature of box 3, and the same inequality holds for the salinities, the main reason being that box 1 receives directly the warm and salty tropical water. In this equilibrium state boxes 1 and 3 receive a net poleward oceanic heat advection of $\approx 1.58\ PW$, and $\approx 0.17\ PW$ respectively: while the former agrees reasonably well with estimates, the latter does not, because the South Atlantic has a weak equatorward flux [Macdonald and Wunsch 1996]. This mistaken sign implies that our model will not be able to capture any dephasing between northern and southern hemisphere high latitudes temperature signals due to changes in the THC strength as those occurred in the past [Blunier et al. 1998, Vidal et al. 1999, Stocker 2000, Stocker 2002]. We underline that nevertheless in our model we observe such dephasing when we obtain the reversal of the THC, because we have a cooling of the northern Atlantic box and a corresponding warming of the southern Atlantic box. Taking into account equation 1.9 and considering that the actual equilibrium q is positive, we conclude that the THC is haline-dominated: the ratio between the absolute value of the thermal and of the haline contribution on the right side of equation 1.9 is ≈ 0.8. We report in table A.1 the value of the main model constants, while in table A.2 we present the fundamental parameters characterizing this equilibrium state.

2.2 Feedbacks of the system

The newtonian relaxation law for the temperature implies that the atmosphere has a negative thermic feedback:

- T_1 increases more than $T_3 \Rightarrow H_1$ decreases more than $H_3 \Rightarrow T_1$ decreases more than T_3

Apart from the mean flow feedback, the reaction of the ocean to a decrease in the value of the THC is depicted in figure 2-1, where the symbol (') indicates that we are

dealing with small perturbations from the equilibrium value of the quantity which the prime sign is referred to, and can be described as follows:

- q decreases $\Rightarrow$

1. T_1 decreases more than T_3 $\Rightarrow$

   (a) the change is limited by the Atmospheric feedback;

   (b) q increases;

2. S_1 decreases more than S_3 $\Rightarrow$ q decreases;

Generally the fe
even if it trigger

$$
q' < 0 \Rightarrow \begin{cases} -(\text{Atmospheric Feedback}) \\ \Uparrow (1a) \\ 1) \Rightarrow T_1' < T_3' < T_2' \\ \Downarrow (1b) \\ q' > 0 \quad (-) \\ \\ \\ 2) \Rightarrow S_1' < S_3' \\ \Downarrow (2) \\ q' < 0 \quad (+) \end{cases}
$$

Figure 2-1: Feedbacks scheme of the uncoupled model (Mixed BCs)

the strength of the second order feedback mechanism $1b$ is relevant in establishing the overall stability of the THC [Tziperman et al. 1994]; a very strong temperature-restoring atmospheric feedback like that in our model tends to decrease the stability of the system [Nakamura et al. 1994, Rahmstorf 2000]. The feedbacks (1) + (2) are governed by q, so that their time scale is around the flushing time of the oceanic boxes; a fast perturbation avoids those feedbacks.

We perform two sets of experiment in order to simulate global warming conditions.

In the first, we increase the freshwater fluxes into the two high-latitude boxes. The rationale for this forcing is in the fact that an increase in the global mean temperature

produces an increase in the moisture capacity of the atmosphere, and this is likely to cause the enhancement of the hydrological cycle, and especially in the transport of moisture from the tropics to the high latitudes. We will explicitly explore this effect in greater detail in chapter 4, where we consider the coupling between the atmosphere and the ocean.

In the second, we represent the purely thermic effects of global warming by setting the increase in the target temperatures of the two high-latitude boxes larger than that of the tropical boxes, since virtually all GCM simulations forecast a larger increase in temperatures in the high latitudes (the so-called *polar amplification*).

2.3 Freshwater flux forcing

We force the previously defined equilibrium state with a net freshwater flux into the two high latitudes boxes which increases linearly with time. This is obtained by prescribing:

$$F_i(t) = \begin{cases} F_i(0) + F^t_{i=1,3} \cdot t, & 0 \leq t \leq t_0, \quad i = 1,3 \\ F_i(0) + F^t_{i=1,3} \cdot t_0 & t > t_0, \quad i = 1,3. \end{cases} \tag{2.2}$$

When the perturbation is over, we reach a final state that can be either qualitatively similar to the initial northern sinking equilibrium or radically different, i.e. presenting a reversed THC. We underline that we impose that the freshwater conservation equation 1.7 holds at all times, so that while we change F_1 and F_3, we also suitably change F_2. We have that each perturbation can be uniquely specified by a set of three parameters, such as the triplet 1 $[t_0, \Delta F_3/\Delta F_1, \Delta F_1]$, or the triplet 2 $[t_0, \Delta F_3/\Delta F_1, F_1^t]$, where $\Delta F_i \equiv F_i^t \cdot t_0$, $i = 1,3$. In order to describe a global warming scenario, we explore the effect of positive ΔF_1 and ΔF_3. Freshwater forcing into box 1 tends to destabilize the THC, since it induces a freshening and so a decrease of the density of the water there contained; the converse holds for increases in the net freshwater flux into box 3 (see 1.11). If the freshwater forcing is larger in the box 3, we cannot obtain a reversal of the THC, so that we limit ourselves to the case $\Delta F_3/\Delta F_1 < 1$. These perturbations cause an initial decrease in the THC strength q and so trigger the oceanic feedbacks described in figure 2-1:

- F_1's increase larger than F_3's $\Rightarrow$ S_1 decreases more than S_3 $\Rightarrow$ q decreases.

We present in figure 2-2 two trajectories of q describing the evolution of the system from the initial equilibrium state when two different forcings, one subcritical and one

ings. In figure 2-3 we observe that, as expected, for a given ΔF_1, the lower is the value of the ratio $\Delta F_3/\Delta F_1$, the lower is the total change ΔF_1 needed to obtain the reversal of the THC. For a given value of the ratio $\Delta F_3/\Delta F_1$, more rapidly increasing perturbations (larger F_1^t) are more effective in disrupting the circulation. For values of $\Delta F_3/\Delta F_1 \leq 0.4$ we see a changeover between a *slow* and a *fast* regime, geometrically described by a relatively steep portion dividing two portions of the manifold having little t_0-dependence. Figure 2-4 shows more clearly that for large values of $\Delta F_3/\Delta F_1$ (≥ 0.5) the collapse of the THC occurs only for fast increases, because of the presence of a threshold in the rate of increase depicted by the little t_0-dependence of the manifold. The changeover corresponds to $t_0 \approx 250\ y$, which essentially matches the flushing time of the oceanic boxes [Scott et al. 1999]. For low values of $\Delta F_3/\Delta F_1$ the transition takes place even in the case of a very low F_1^t because, as shown in the bifurcation analysis performed by [Scott et al. 1999], there is a critical ratio $\Delta F_3/\Delta F_1$ below which the northern sinking equilibrium becomes unstable: such a ratio can be reached after a long enough t_0 if $\Delta F_3/\Delta F_1$ is low enough.

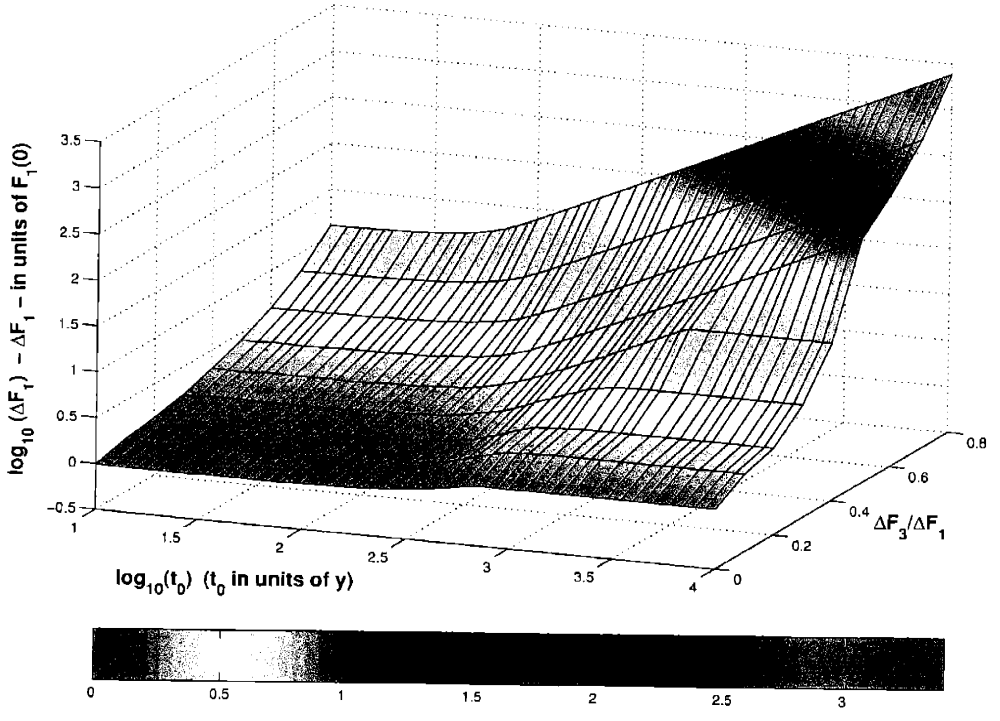

Figure 2-3: Critical values of the total increase of the freshwater flux - Uncoupled Model (Mixed BCs)

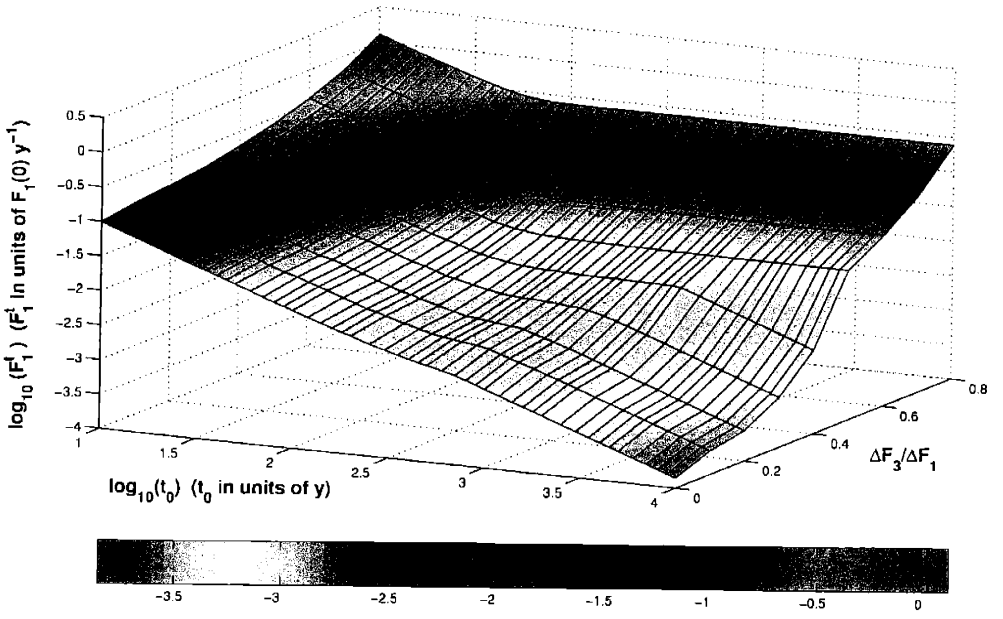

Figure 2-4: Critical values of the rate of increase of the freshwater flux - Uncoupled Model (Mixed BCs)

2.3.2 Bifurcation

In figure 2-5 we present the bifurcation diagrams describing the stability of this model to a slow freshwater flux forcing applied in both boxes 1 and 3; in this case we apply quasi-static perturbations, i.e. t_0 is very large. We show 5 loops, corresponding to $\Delta F_3/\Delta F_1 = [0, 0.1, 0.2, 0.3, 0.4]$. For a given curve, each point (x, y) plotted represents a stable state of the system having $q = y$ and $F_1 = x$. We scale all the graphs so that the common initial equilibrium state is the point $(1, 1)$. For a range of F_1, which depends on the value of $\Delta F_3/\Delta F_1$, the system is bistable, i.e. it possesses two distinct stable states, one having $q > 0$, the other one having $q < 0$. The history of the system determines which of the two stable states is realized. The boundaries of the domain in F_1 where the system is bistable correspond to subcritical Hopf bifurcations, which drive the system from the northern (southern) sinking equilibrium to the southern (northern) sinking equilibrium if F_1 crosses the right (left) boundary of the domain of bistability. As previously explained if $\Delta F_3/\Delta F_1$ is large enough (≥ 0.5) slow increases of the freshwater fluxes do not destabilize the system, so that no bifurcations are present. The presence of an hysteresis for slow freshwater flux perturbations has been presented both for simple [Rahmstorf 1995, Rahmstorf 1996, Scott et al. 1999, Titz et al. 2002a] (albeit with

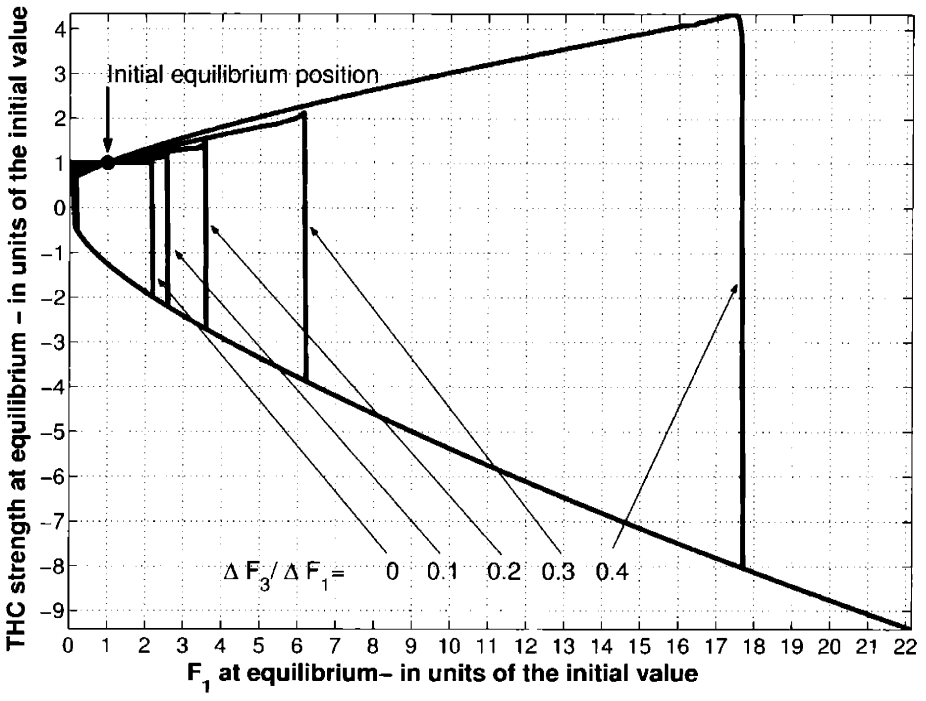

Figure 2-5: Bifurcation diagram of freshwater flux forcings - Uncoupled model (Mixed BCs)

differences in the model formulation in some cases) as well as more complex inter-hemispheric models [Stocker and Wright 1991, Mikolajewicz and Maier-Reimer 1994, Rahmstorf 1995, Rahmstorf 1996]; the inclusion of changes in the freshwater flux into both high latitudes boxes presented in this work had not been previously explicitly considered.

2.4 Heat flux forcing

We explore the stability of the northern sinking equilibrium against perturbations to the initial heat fluxes expressed as changes in the target temperatures in the three boxes. We do not impose a constraint fixing the average target temperature τ_M, so that in this case not two but three parameters τ_1, τ_2, τ_3 can be changed. It is possible to recast the system equations 1.1−1.6 [Scott et al. 1999] so that the heat forcing is described completely by the changes in $\tau_N = \tau_1 - \tau_2$ and in $\tau_S = \tau_3 - \tau_2$. Therefore we set $\tau_2 = \tau_2(0)$ at all times, so that $\tau_1^t = \tau_N^t$ and $\tau_3^t = \tau_S^t$. We apply the following

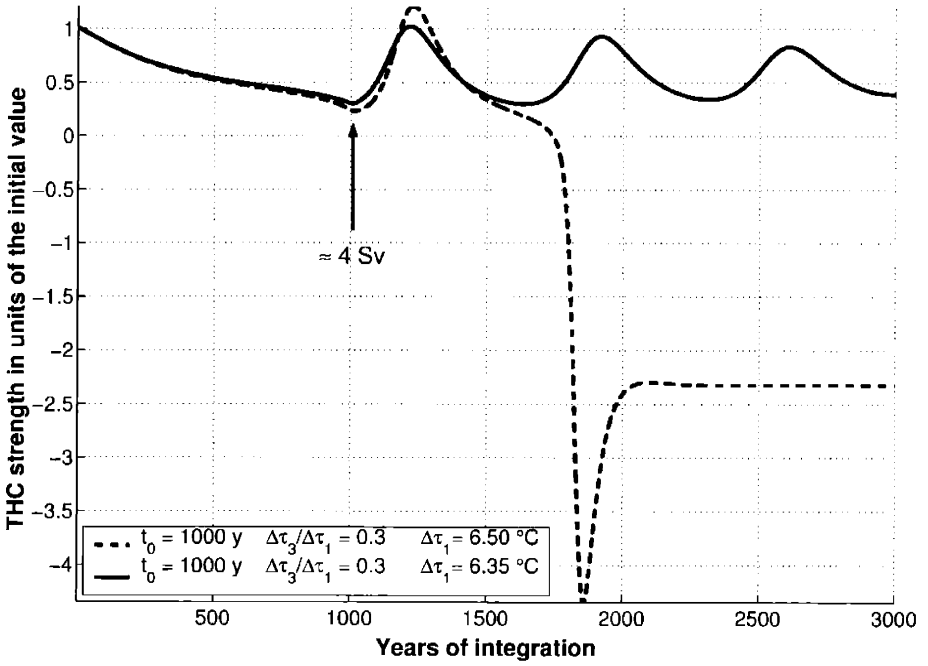

Figure 2-6: Evolution of the THC strength under a super- and sub-critical forcing to target temperatures - Uncoupled Model (Mixed BCs)

forcings:

$$\tau_i(t) \quad = \quad \begin{cases} \tau_i(0) + \tau_i^t \cdot t, & 0 \leq t \leq t_0, \quad i = 1,3 \\ \tau_i(0) + \tau_i^t \cdot t_0 & t > t_0, \quad i = 1,3 \end{cases} \tag{2.3}$$

We characterize each forcing experiment, which leads to a final state that is characterized by a northern or a southern sinking equilibrium, using the parameter set 1 defined as $[t_0, \Delta\tau_3/\Delta\tau_1, \Delta\tau_1]$ and the parameter set 2 defined as $[t_0, \Delta\tau_3/\Delta\tau_1, \tau_1^t]$; consistently with the previous case we define $\Delta\tau_i \equiv \tau_i^t \cdot t_0$, that is the total change of the target temperature of the box i. In order to imitate global warming scenarios where polar amplification occurs, we consider $\Delta\tau_i \geq 0$, $i = 1,3$. We observe that if $\Delta\tau_3 > \Delta\tau_1$, no destabilization of the THC can occur, because such a forcing reinforces the THC. The specified forcings trigger the previously described feedbacks of the system in the following way:

- τ_1's increase larger than τ_3's $\Rightarrow$ H_1's increase larger than H_3's $\Rightarrow$ T_1 increases more than T_3 $\Rightarrow$ q decreases $\Rightarrow$ feedbacks in Figure (2).

We present in figure 2-6 two trajectories of q starting from the initial equilibrium state, characterized by slightly different choices of the forcing applied to τ_1 and τ_3. One of the forcing is supercritical, the other one is subcritical. The two trajectories are barely

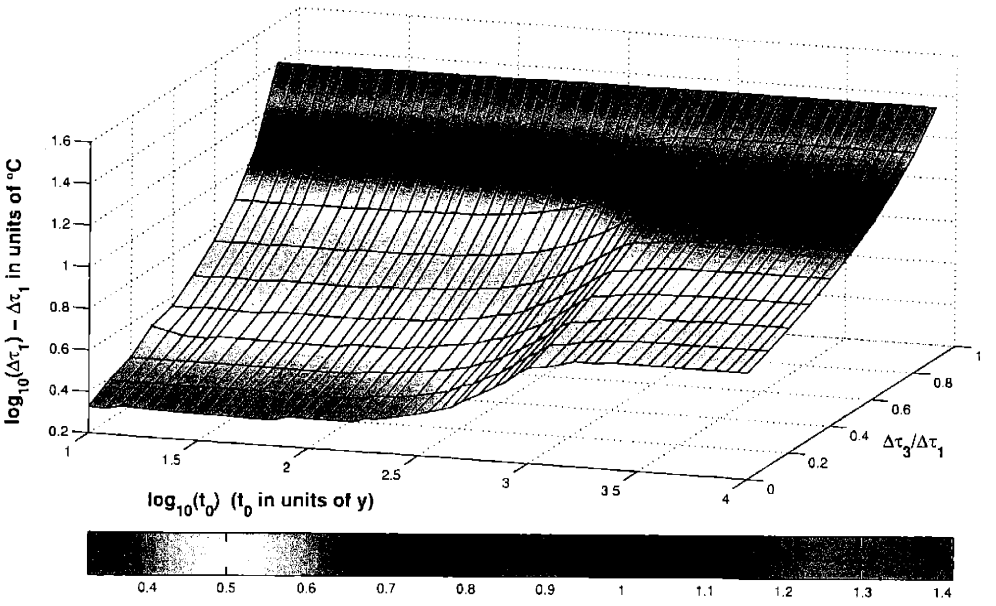

Figure 2-7: Critical values of the total increase of the target temperatures - Uncoupled Model (Mixed BCs)

distinguishable up to the end of the perturbation, because the forcing dominates the internal feedbacks of the system thanks to the large value of λ (although we notice that after around 400 years the decrease of q slows down); the mean flow feedback dampens the increase in T_1 and keeps the system in the northern sinking state, although the decreasing q lowers the amount of warm, salty tropical water injected into box 1; when q gets too small (in this case about 4 Sv) the mean flow feedback becomes negligible and the system eventually collapses. The period of the oscillations is comparable with the time scale of the flushing of the oceanic boxes.

2.4.1 Critical Forcings

Figures 2-7 and 2-8 present, using respectively the parameter sets previously designated with 1 and 2, the manifold of the critical forcings. In figure 2-7 we can observe that for all the values of $\Delta\tau_3/\Delta\tau_1$ there is a steep portion of the manifold (corresponding to a time scale of $\approx 250\ y$) dividing two flat regions describing the *fast* and *slow* regimes. In the fast region, a smaller total increase $\Delta\tau_1$ is required to achieve the reversal of the THC. For $\Delta\tau_3/\Delta\tau_1 = 0.9$, which represents the case of highly symmetrical forcings, the critical $\Delta\tau_1$ essentially does not depend on t_0. The absence of thresholds in τ_1^t in the case of more symmetric forcing (large $\Delta\tau_3/\Delta\tau_1$) is clear in

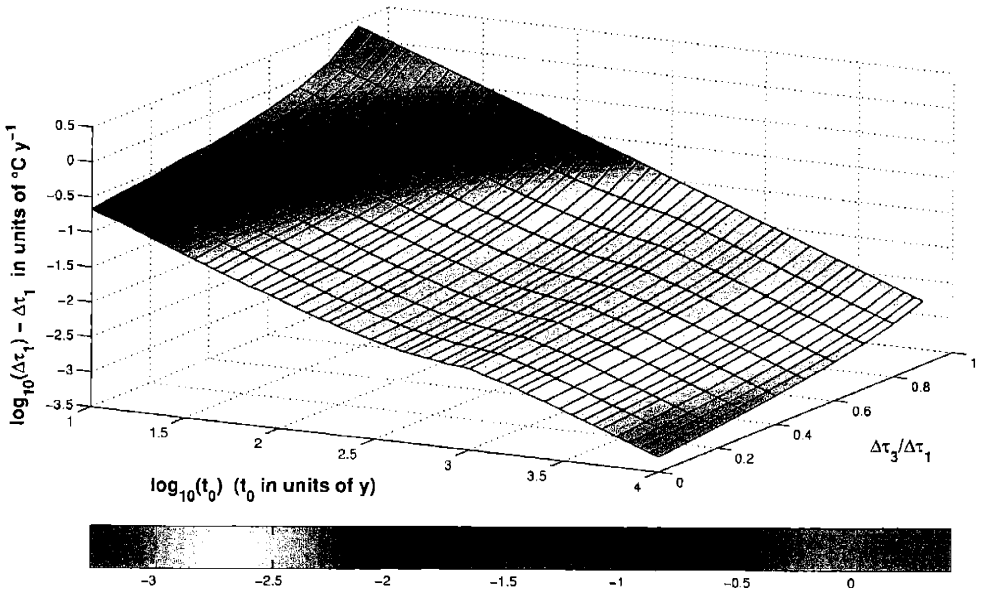

Figure 2-8: Critical values of the rate of increase of the target temperatures - Uncoupled Model (Mixed BCs)

figure 2-8: no flat regions, like those encountered in figure 2-4, can be found. The main reason for this property of the system's response to perturbations to the target temperatures, is that because of the large value of λ, which is about one order of magnitude larger than the initial q, the forcing is stronger than any negative feedback. If the increase in τ_1 is slow enough, the negative feedbacks make the destabilization more difficult, but do not prevent it.

2.4.2 Bifurcations

For this class of forcings, the achievement of the collapse of the THC is not restricted by any threshold on the rate of increase, therefore we expect the presence of bifurcations for every ratio of $\Delta\tau_3/\Delta\tau_1 < 1$. We present in figure 2-9 only the graphs relative to $\Delta\tau_3/\Delta\tau_1 = [0, 0.2, 0.5, 0.6, 0.8]$ for sake of simplicity; the other curves that can be obtained for other values of $0 \leq \Delta\tau_3/\Delta\tau_1 < 1$ are not qualitatively different. The initial state is the point $(0, 1)$. The subcritical Hopf bifurcation points are respectively $(\approx 5, \approx 0.7)$, $(\approx 6, \approx 0.7)$, $(\approx 9, \approx 0.7)$, $(\approx 13, \approx 0.7)$ and $(\approx 17, \approx 0.5)$, which means that the bifurcation occurs when the THC has already declined down to ≈ 10 Sv. The bistable region is extremely large in all cases, because the x of the bifurcation points in the lower part of the circuits are below $-50°C$; they become farther

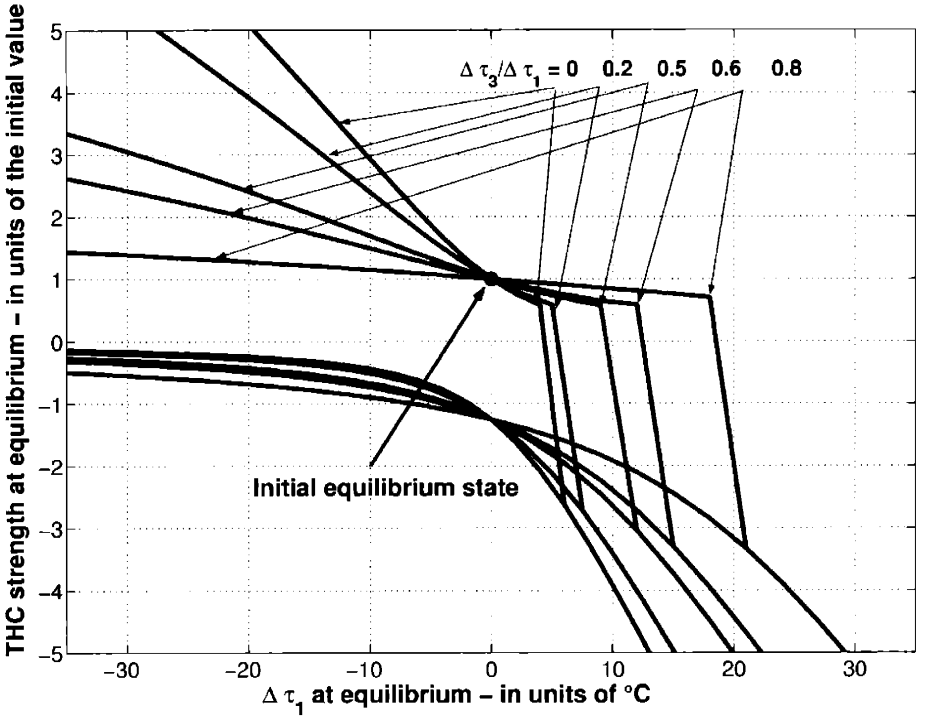

Figure 2-9: Bifurcation diagram of the target temperature forcings - Uncoupled model (Mixed BCs)

and farther from the initial equilibrium value as $\Delta\tau_3/\Delta\tau_1$ increases. This means that once the circulation has reversed, the newly established pattern is extremely stable and can hardly be changed again. To our knowledge, this is the first time such an analysis of bifurcation for this class of forcing is presented.

Chapter 3

Uncoupled Model with Flux Boundary Conditions

3.1 Main features of this version of the model

In the second version of the model we replace the expression of the heat flux in the box i defined in the previous model as $\lambda(\tau_i - T_i)$ with a free parameter H_i. Choosing the value of the initial H_i equal to the value of $\lambda(\tau_i - T_i)$ of the previous version of the model at equilibrium, we obtain the same equilibrium solution. Therefore this model has flux boundary conditions on both temperature and salinity variables. We then perturb this equilibrium solution with freshwater flux forcing

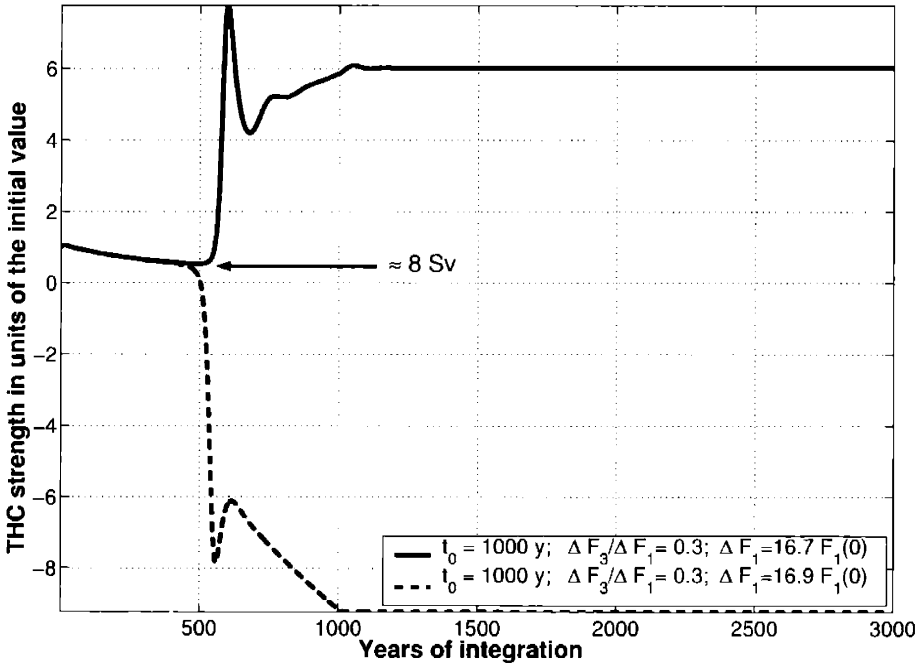

Figure 3-1: Evolution of the THC strength under a super- and sub-critical freshwater flux forcing - Uncoupled Model (Flux BCs)

as in the previous case, and with explicit heat flux forcing. Since the heat flux H_i does not depend on T_i, so that our restoring time is infinite, the positive feedback (1*b*) described at the beginning of the section is off, therefore we expect this version of the system to be more stable than the previous one, in agreement with the results of [Tziperman et al. 1994, Nakamura et al. 1994, Rahmstorf 2000], who have found that stability is enhanced when the temperature restoring times increases. The absence of this feedback, which implies that heat fluxes changes generate global radiative imbalances that never recover, makes this version less realistic in representing the true climate system, but because of the possibility of applying specific heat flux perturbations, it is possible to compare directly in terms of efficacy in destabilizing

the system the heat flux and the freshwater flux perturbations, expressing both in equivalent density units. We observe that in this version of the model the prognostic equation for q previously presented can be directly verified when the system is at equilibrium.

3.2 Freshwater flux forcing

We follow exactly the same procedure delineated in the previous subsection describing freshwater flux perturbations. In figure 3-1 we present the effects on q of two similar forcings involving changes in F_1 and in F_3, one of which is subcritical and the other is supercritical. We use the same length of increase and the same asymmetry in the

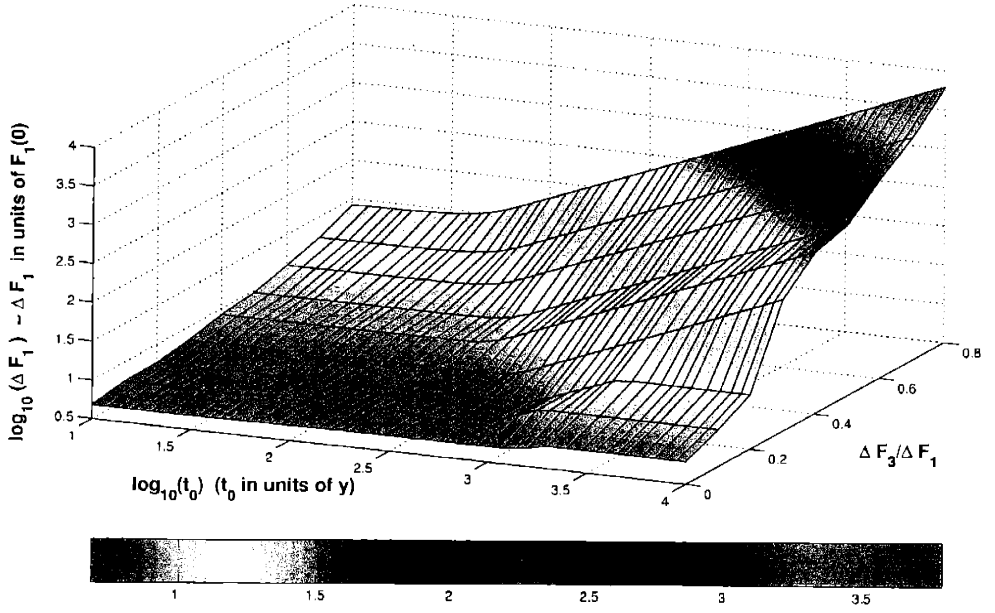

Figure 3-2: Critical values of the total increase of the freshwater flux - Uncoupled Model (Flux BCs)

forcing as in the mixed boundary conditions: we observe that the total change of F_1 needed to obtain the collapse of the THC is about 3 times larger. We observe that even if the total length of the perturbation is 1000 years, the separation of the two trajectories of q takes place around 500 y after the start of the forcing. We then observe oscillations with period of the order of 200 years, due to the negative feedback related to the flushing of the oceanic boxes. The threshold value for q is, as in the case of mixed boundary conditions, of the order of 10 Sv.

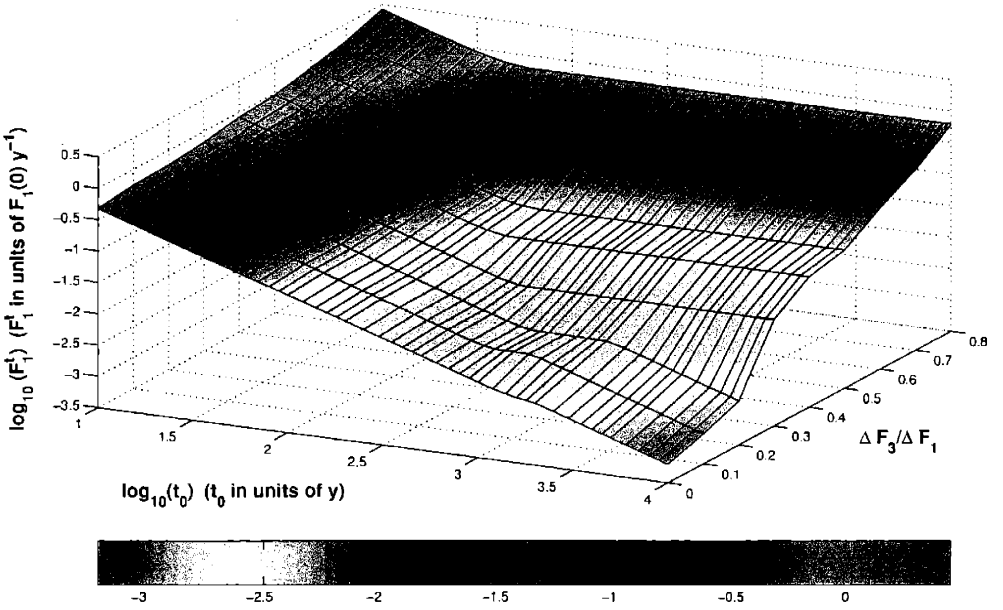

Figure 3-3: Critical values of the rate of increase of the freshwater flux - Uncoupled Model (Flux BCs)

3.2.1 Critical Forcings

Figures 3-2 and 3-3 presents the manifold of the critical perturbations using respectively the coordinate system $[t_0, \Delta F_3/\Delta F_1, \Delta F_1]$ and $[t_0, \Delta F_3/\Delta F_1, F_1^t]$. While the main features of figure 3-2 resemble those of figure 2-3, the enhanced stability of the system is shown by the larger value of total change ΔF_1 needed to disrupt the THC for a given choice of ΔF_1 and $\Delta F_3/\Delta F_1$. Figure 3-3 shows that in the domain in the $\Delta F_3/\Delta F_1$ direction allowing collapse of the THC also for indefinetely slow increases is smaller than in the mixed BCs: if $\Delta F_3/\Delta F_1 > 0.2$ there is a threshold in the rate of theforcing. Figure 3-4 shows the ratio between the values of the critical values of ΔF_1 presented in figure 2-3 and the corresponding values obtained with the flux BCs model and presented in figure 3-2. The average value of this ratio over all the domain is ≈ 0.3. Observing figure 3-4 for the $\Delta F_3/\Delta F_1$ values $[0.3, 0.4]$, we see that the ratio goes to 0 with increasing t_0. This occurs because for these values the threshold in the rate of increase is present only in the flux BCs model, therefore in this model for large t_0 the quantity ΔF_1 diverges, while in the mixed BC model it is finite.

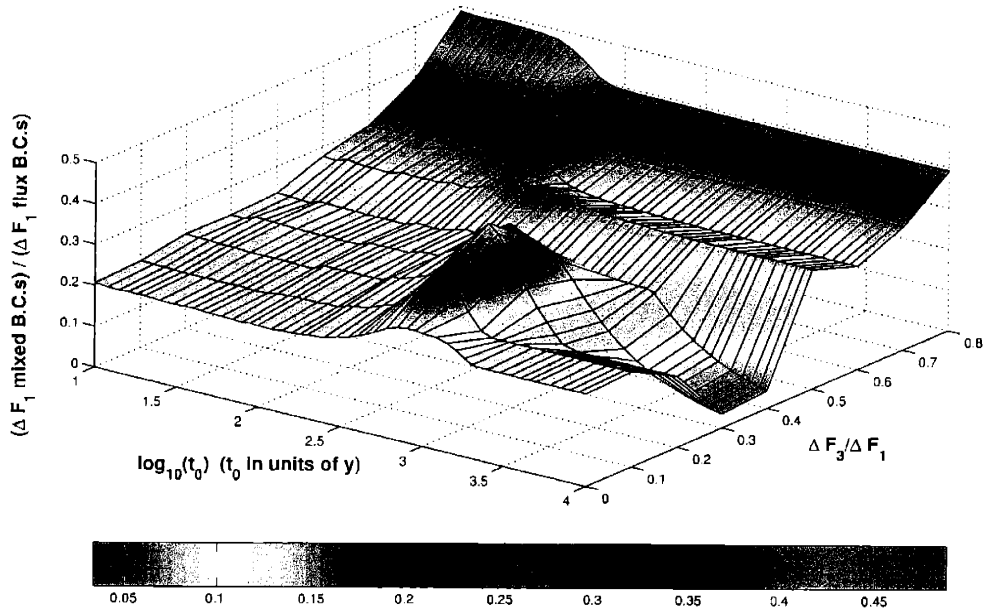

Figure 3-4: Comparison between the stability of the mixed and flux BCs uncoupled model to increases of the freshwater flux

3.2.2 Bifurcations

In figure 3-5 we present the bifurcation diagrams describing the stability of this version of the model to a slow freshwater forcing applied in both boxes 1 and 3 for $\Delta F_3/\Delta F_1 = [0, 0.1, 0.2]$ in comparison with the results obtained with the mixed BC's model in figure 2-5. Also in this case we obtain hysteresis graphs describing the presence of a domain of bistability, and, as in the case of mixed boundary conditions, the transitions between northern and southern sinking equilibrium and vice versa take place at subcritical Hopf bifurcations. It is apparent that the version of the model here analyzed is more stable to freshwater flux perturbations than the mixed boundary conditions model. In this case no bifurcations are present for $\Delta F_3/\Delta F_1 = [0.3, 0.4]$, while for each of the cases $\Delta F_3/\Delta F_1 = [0, 0.1, 0.2]$ the bifurcation point is much farther than in the mixed boundary conditions model from the point $(1, 1)$, which describes the unperturbed system.

3.3 Heat flux forcing

Using the same arguments of the corresponding part of the previous section, we can prove that the relevant variables of the system are the differences between the values

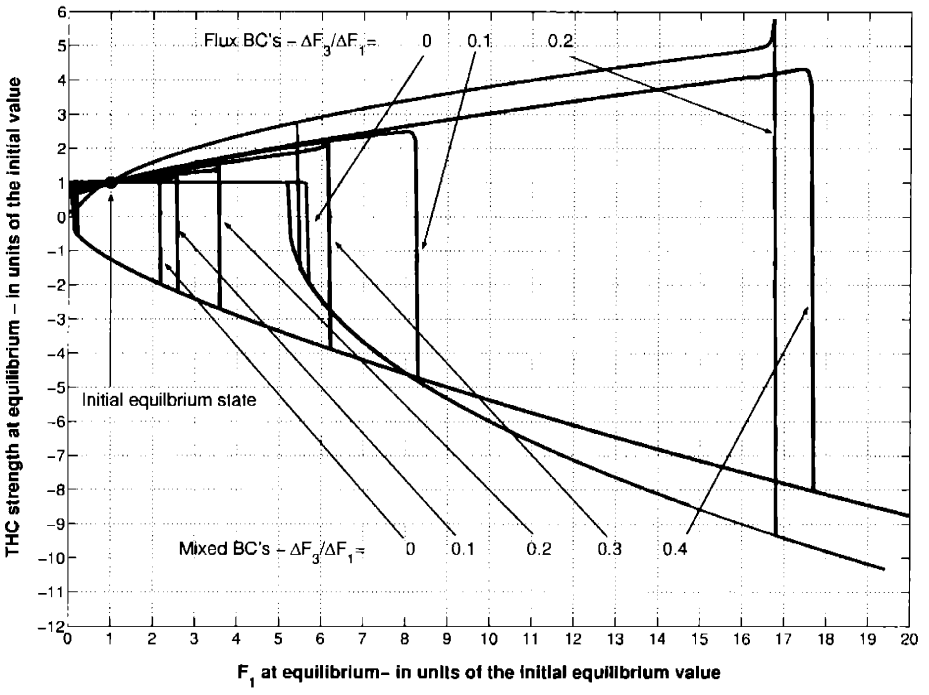

Figure 3-5: Bifurcation diagram of freshwater flux forcings - Mixed (blue lines) and Flux BCs (red lines) uncoupled models

of the salinity and of the temperature between the two high-latitude boxes and the tropical box, so that in this context the parameters to be changed are $H_N = H_1 - H_2$ and $H_S = H_3 - H_2$. We set $H_2 = H_2(0)$, so that the perturbations to H_N (H_S) are respectively equal to the perturbations to H_1 (H_3). We then prescribe the following time-dependence of H_1 and H_3:

$$H_i(t) = \begin{cases} H_i(0) + H_i^t \cdot t, & 0 \leq t \leq t_0, \quad i = 1,3 \\ H_i(0) + H_i^t \cdot t_0 & t > t_0, \quad i = 1,3 \end{cases} \tag{3.1}$$

Following the argument developed for the thermal forcing in the mixed boundary conditions mode, we consider $\Delta H_i \geq 0$, $i = 1,3$, and $\Delta H_3 / \Delta H_1 < 1$, where we have defined $\Delta H_i \equiv H_i^t \cdot t_0$, $i = 1,3$. When the forcing to the heat fluxes stops, the system is in positive radiative imbalance, so that its average temperature will increase indefinitely. In figure 3-6 we present the effects of two similar forcings, one subcritical and one supercritical on the strength of the THC. In this case there is no positive threshold in the value of q, i.e. the THC recovers from a whichever low positive value. The reason for this behavior is that the tropical box, in a regime of low q, gets very warm and very salty, (both its negative freshwater flux budget and its positive heat flux budget remain unchanged), but for the very reason the circulation

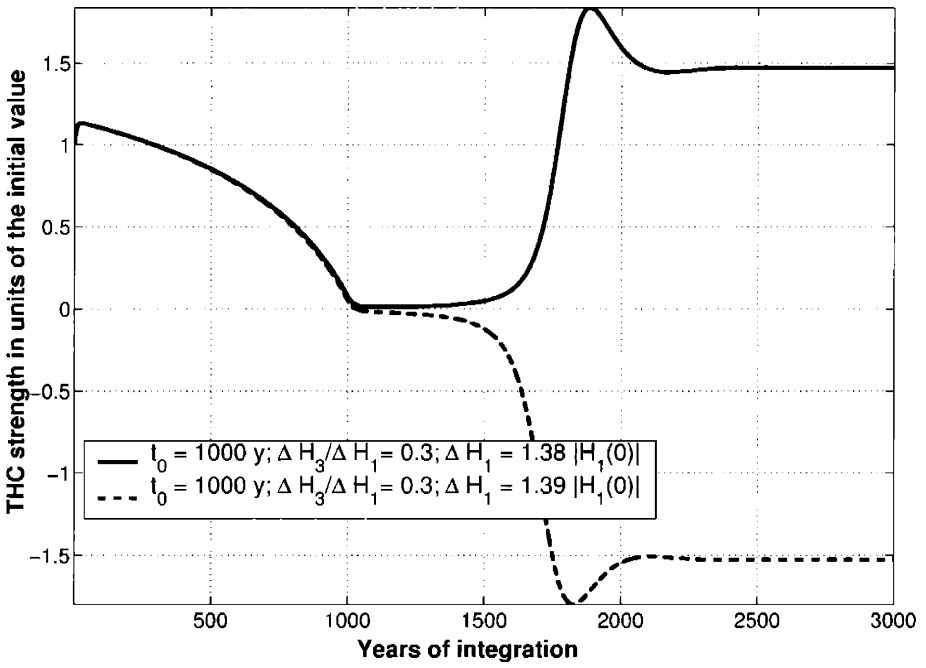

Figure 3-6: Evolution of the THC strength under a super- and sub-critical heat flux forcing - Uncoupled Model (Flux BCs)

is haline-dominated, the net effect is a large increase of its density. Therefore as soon as the forcing stops, there is a large oceanic flux of density into box 1, that generates a positive feedback which drives up the value of q. The eventual stabilization of the THC requires that the system reaches a dynamic equilibrium, in which the global average temperature steadily grows. In such an equilibrium equation 1.8 is *not* satisfied. We point out that if H_3/H_1 is very small, the THC asymptotically goes to zero and never recovers for subcritical perturbations, while it dies away after having reversed for weakly supercritical perturbations: in absence of a THC the system behaves unphysically since the constant freshening of the two high latitude boxes drives their salinity to negative values [Rooth 1982, Scott et al. 1999].

3.3.1 Critical Forcings

Figures 3-7 and 3-8 show the manifold of the critical forcings, using respectively the coordinates $[t_0, \Delta H_3/\Delta H_1, \Delta H_1]$ and the coordinates $[t_0, \Delta H_3/\Delta H_1, H_1^t]$. They qualitatively look similar to figures 2-3 and 2-4 respectively, and similar remarks can be made, the main difference being that we can deduce from figure 3-8 that the threshold in the rate of increase is present only if $\Delta H_3/\Delta H_1 \geq 0.6$, while in the case of freshwater flux perturbations the threshold in the rate of increase of

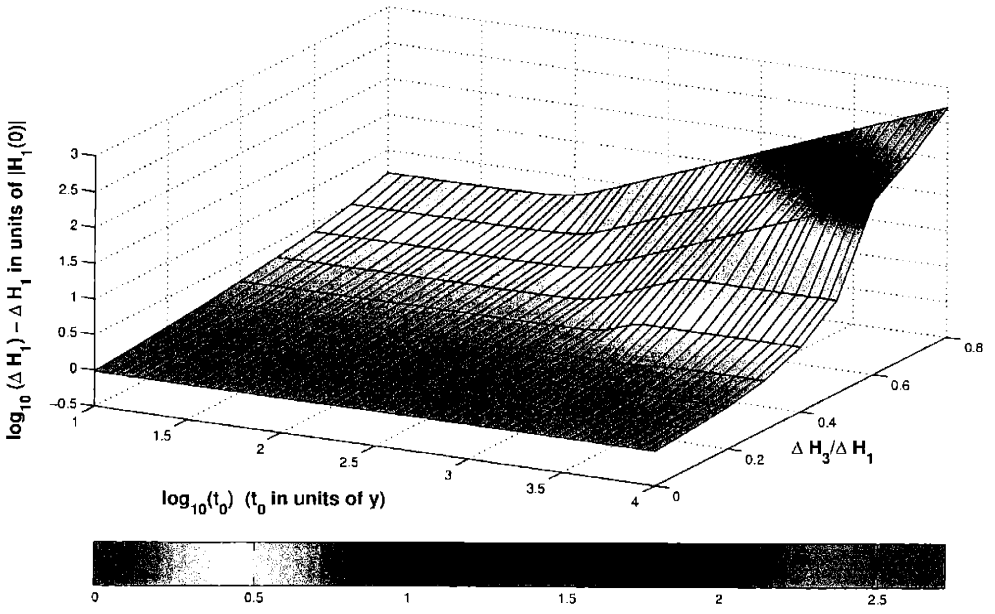

Figure 3-7: Critical values of the total increase of the heat flux - Uncoupled Model (Flux BCs)

the forcing is present also for geographically much more asymmetric forcings. The essentially equivalent formulation of the heat and freshwater fluxes in this version of the model allows an interesting comparison between the effectiveness of heat and freshwater flux increases in destabilizing the system, which was not possible in the mixed boundary conditions case since at any time the heat flux H_i depends also on the actual local temperature T_i. In order to do that, we express the heat flux changes in equivalent freshwater flux changes multiplying the former times the factor α/β. Rescaling the manifolds of the critical forcings in the same density units, we can directly compare it with the manifold obtained in the study of freshwater flux perturbations. Moreover, since the THC is density-driven in our model and does not discriminate between temperature and salinity-induced changes in the density, one should expect the effectiveness of the thermic and saline perturbations should coincide within a certain parameters' range. We present a comparison between the efficacy of the freshwater and the heat flux perturbations in destabilizing the system in figure 3-9. In this figure ratio between the rescaled heat flux H_1 and the freshwater flux F_1 leading to the collapse of the THC is plotted against the length of the forcing and the ratio between the forcing applied in the southern and in the northern high latitude boxes. This figure shows that when expressed in the same units, the two manifold

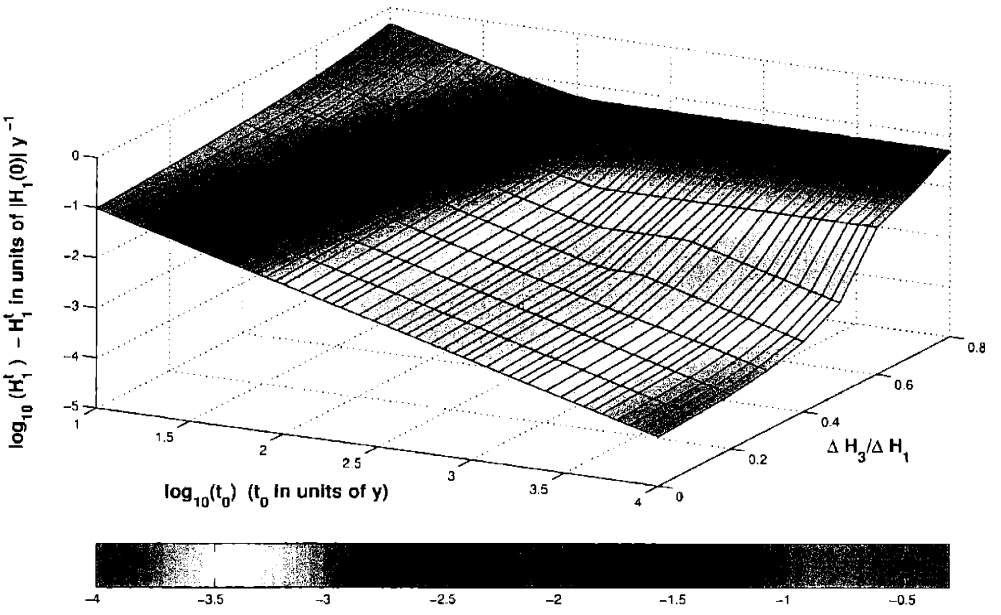

Figure 3-8: Critical values of the rate of increase of the heat flux - Uncoupled Model (Flux BCs)

presented in figures 3-2 and 3-7 coincide remarkably well if the increases are fast, while for slow increases the heat flux perturbations are more effective in destabilizing the THC. The portion where the two manifolds coincide becomes narrower and narrower as the ratios $\Delta H_3/\Delta H_1$ and $\Delta F_3/\Delta F_1$ increase. The larger effectiveness of the thermic destabilization is due to the fact that while the average salinity is always a conserved quantity, so that slow increases of the freshwater flux F_1 can be strongly counteracted by the negative feedback of the mean flow, the average temperature is not a conserved quantity in the heat fluxes H_i are perturbed, so that the mean flow feedback is less effective for increases in H_1.

3.3.2 Bifurcation

Since in this set of experiments we do not obtain at the end of the forcing an equilibrium, because the radiative imbalance persists, it is not possible to define a bifurcation diagram as in the previous cases. Nevertheless we present in figure 3-10 the graph portraying the value of q obtained by changing slowly the value of the H_1 (H_2 and H_3 are kept constant at the initial value) along the paths indicated by the arrows, in order to obtain information on the stability properties of the system. From the initial state $(-1, 1)$, where the sign is taken accordingly with the fact that the initial H_1 at

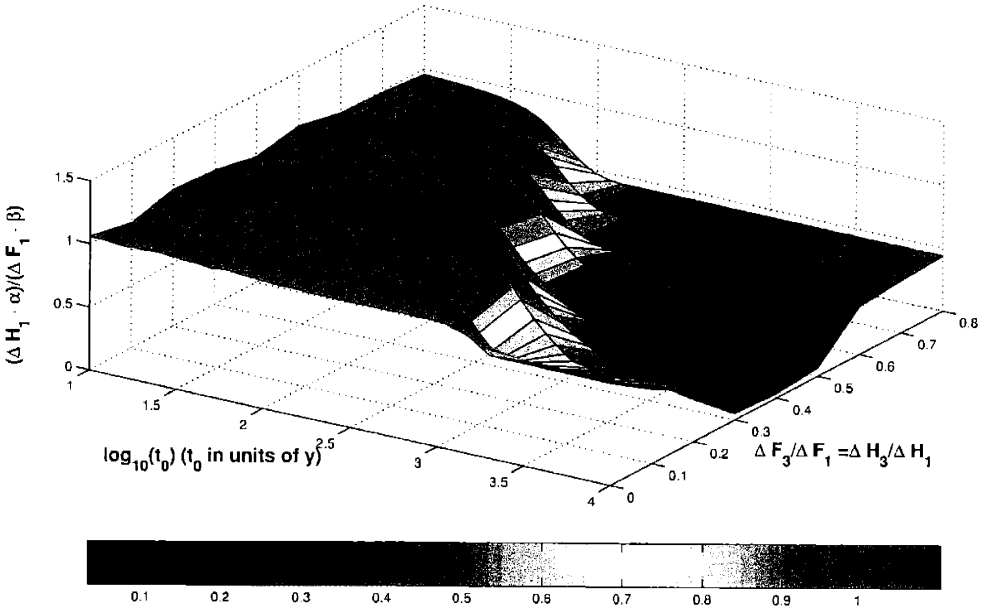

Figure 3-9: Comparison between the relative efficacy of freshwater vs. heat flux increases in destabilizing the warm mode of the THC - Uncoupled Model (Flux BCs)

equilibrium is negative, we first increase H_1 until we obtain the reversal of the THC; we then decrease H_1 until the northern sinking state is recovered; we then increase H_i again to close our circuit; the circuit closes at $y = q = 0$. We observe that the initial point $(-1, 1)$ is within the upper and the lower branches of the circuit. This is the case because the closed, external path described by the arrows strictly contains all the possible evolutions of the system for quasi static changes in H_1. We mean that if the sign of the change of H_1 is reversed (with respect to what indicated by the arrows in figure 3-10) when the system is in a portion of the external circuit where an upper and a lower branches are present, the point representing the system does not go along the previously followed path in the opposite verse, but moves inside the space between the upper and the lower branches. Qualitatively this behavior resembles what we obtain when we measure the intensity of the magnetic field inside a paramagnetic body subject to a slowly varying external magnetic field. The sense of such a parallel is in the fact that in these sets of experiments the heat flux plays the role of a wholly external parameter, since no global conservation law applies.

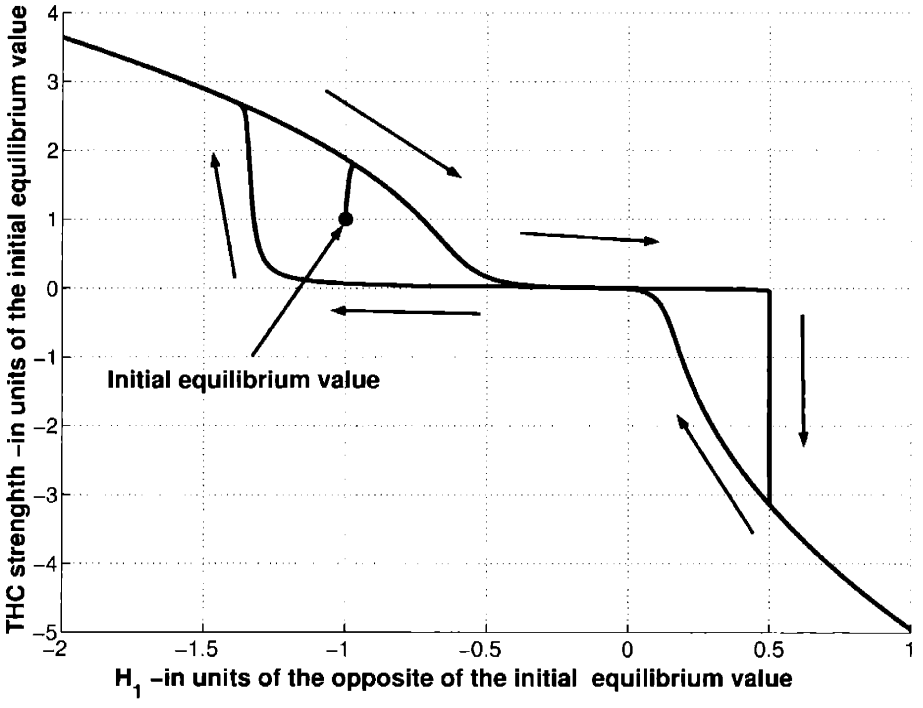

Figure 3-10: Variation of THC to quasi-static changes of H_1 - Uncoupled Model (Flux BCs)

Chapter 4

Coupled Atmosphere-Ocean Model

4.1 Physical properties of the coupled model

This version of the model closely follows Scott et al. [Scott et al. 1999] model except for the addition of the effect of the Clausius-Clapeyron equations on moisture and latent heat transport; it differs greatly from the models presented in the previous chapters since it incorporates explicit coupling between the ocean and the atmosphere. The coupled model is such that the main atmospheric physical processes responsible for freshwater and heat fluxes have distinct formulations, therefore the simulation of global warming scenarios can be obtained more realistically by forcing the radiative flux term alone. In the coupled model the atmosphere has a negligible heat capacity and water content compared to the ocean, and its only function is to serve to transport heat and moisture; for time scales longer than a few months this is a reasonable approximation [Gill 1982]. The land is also assumed to have negligible heat capacity and water content. The oceanic boxes $i = 1, 3$ receive a fraction $1/\gamma_i$ of the total net moisture transported by the atmosphere from the box 2 to the boxes $i = 1, 3$; this includes the fraction that directly precipitates over the oceanic boxes $i = 1, 3$ and the fraction that precipitates over land and runs off to the oceanic boxes $i = 1, 3$. The fractional catchment area $1/\gamma_i$ can range in our system from 1 (all of the atmospheric moisture exported from the tropics to the latitudes where the oceanic boxes $i = 1, 3$ are ends up respectively in the boxes $i = 1, 3$) to 1/6 (the box $i = 1, 3$ receives only the moisture transported from the tropics that precipitates on the ocean surface). The remaining fraction $(1 - 1/\gamma_i)$ of the total atmospheric moisture exported from the tropics returns back to the oceanic box 2 by river runoff or underground flow. This latter fraction does not effect the moisture budget of the oceanic boxes $i = 1, 3$ but does effect their heat budget, since the process of condensation occurs over the region $i = 1, 3$, so that latent heat is released to the atmosphere and is immediately transferred to the oceanic box $i = 1, 3$. Estimates for γ_i for the Atlantic range from 1.5 to 3 [Marotzke 1996]. We set $\gamma_1 = \gamma_3$ in order to keep the geometry of the problem entirely symmetric, and choose $\gamma_1 = \gamma_3 = 2$.

4.2 Parametrization of the atmospheric fluxes

The rescaled atmospheric fluxes of heat and freshwater in equations 1.1−1.6 are parameterized as functions of the box temperatures T_i. We choose simple but physically plausible functional forms which are based on the large scale processes governing the

transfer of heat and freshwater through the atmosphere. We want to capture the dependence of atmospheric transport from the tropics to the high-latitudes on the temperature gradient, considering that baroclinic eddies contribute for most of the meridional transport around 30 $^{\circ}N$ [Peixoto and Oort 1992], and the dependence of the moisture content of the atmosphere on the average temperature, as well as the dependence of the outgoing long wave radiation on the temperature. The net freshwater fluxes F_i are then parameterized as [Stone and Miller 1980, Stone and Yao 1990]:

$$F_1 = \frac{C_1}{(\frac{T_2+T_1}{2})^3} e^{-\frac{L_v}{R_v \frac{T_2+T_1}{2}}} (T_2 - T_1)^n, \tag{4.1}$$

$$F_3 = \frac{C_3}{(\frac{T_2+T_3}{2})^3} e^{-\frac{L_v}{R_v \frac{T_2+T_3}{2}}} (T_2 - T_3)^n, \tag{4.2}$$

where L_v is the unit mass latent heat of vaporization of water (taken as constant), R_v is the gas constant, and C_1 and C_3 are coefficients we have to calibrate. The exponential functions are derived from the Clausius-Clapeyron law, while the value of the exponent n determines the strength of the temperature gradient feedback; F_2 is obtained using equation 1.7. The surface heat fluxes H_i are decomposed in three components describing physically different phenomena:

$$H_i = SH_i + LH_i + RH_i \tag{4.3}$$

where SH_i and LH_i are respectively the convergence of the atmospheric flux of sensible and latent heat in the box i, while RH_i describes the radiative balance between incoming solar radiation and outgoing longwave radiation. The convergence of atmospheric transports must globally sum up to zero at any time, since the atmosphere is closed. The convergence of the latent heat fluxes LH_i is respectively proportional to the convergence of the freshwater fluxes F_i:

$$\begin{aligned} LH_i &= \gamma_i \frac{L_v}{c_p \cdot S_0 \cdot \rho_0} F_i, \quad i = 1, 3 \\ LH_2 &= -\frac{1}{V}(LH_1 + LH_2) \end{aligned} \tag{4.4}$$

where the constant relating the rescaled freshwater and the latent heat flux has been obtained considering that for the physical fluxes are related by $L\tilde{H}_i = \gamma_i \cdot L_v \cdot \tilde{F}_i$. We note that the Clausius-Clapeyron equations had been included in the description the atmosphere-ocean coupling in earlier studies, but these dealt with hemispheric and not

inter-hemispheric models [Nakamura et al. 1994, Tziperman and Gildor 2002]. We observe that in density units the following relation holds:

$$\left(\frac{LH_i}{F_i}\right)_\rho = \frac{\alpha \cdot \gamma_i \cdot L_v}{\beta \cdot c_p \cdot S_0} \approx 6, \quad i = 1, 3, \tag{4.5}$$

where the lower index in the left hand side denotes that we are dealing with common units. We underline that this value of the ratio depends on the assumptions we have made of the values for γ_i, α and β. For a more realistic equation of state for the density, the ratio could be smaller but is still larger than 1 for a very large temperature range. The convergence of the sensible heat fluxes SH_i are parameterized as a constant times the n^{th} power of meridional temperature gradient [Stone and Miller 1980, Stone and Yao 1990]:

$$\begin{aligned} SH_i &= D_i(T_2 - T_i)^n, \quad i = 1, 3 \\ SH_2 &= -\frac{1}{V}(SH_1 + SH_2) \end{aligned} \tag{4.6}$$

The radiative part RH_i is parameterized as in [Wang and Stone 1980, Marotzke and Stone 1995, Marotzke 1996]:

$$RH_i = A_i - B_i T_i = B_i(\frac{A_i}{B_i} - T_i) = B_i(\vartheta_i - T_i), \quad i = 1, 2, 3. \tag{4.7}$$

With respect to the box i, A_i describes the net radiative budget if $T_i = 0\ ^\circ C$, B_i is an empirical coefficient, which, if albedo is fixed, as in this model, is a measure of the sensitivity of the thermal emissions to space to surface temperature, including also the water vapor and clouds feedbacks, and ϑ_i in the radiative equilibrium temperature.

In order to obtain for the coupled model here presented an equilibrium control solution identical to that of the uncoupled model, we need to carefully choose the constants in the atmospheric parametrization.

4.2.1 Choice of the constants

Using the parametrization proposed in reference [Marotzke 1996], we set for our model $B_1 = B_2 = B_3 = B = 5.1 \cdot 10^{-10}\ s^{-1}$. We can then write for the average temperature T_M of the coupled model an equation similar to 2.1 where B replaces λ and ϑ_M replaces τ_M:

$$\dot{T}_M = B(\vartheta_M - T_M); \tag{4.8}$$

where the parameter B introduces a time scale of ≈ 60 years for the radiative processes; ϑ_i are chosen following the parametrization presented in [Marotzke 1996] and are such that the average radiative temperature $\vartheta_M \equiv (\vartheta_1 + V \cdot \vartheta_2 + \vartheta_3)/(2+V) = \tau_M$. As discussed in the reference [Scott et al. 1999], actually equation 4.8 is more appropriate than equation 2.1 to describe the evolution of the globally averaged temperature of the system, since λ overestimates the effectiveness of global relaxation processes, while well reproducing them box-wise. In physical terms, B correspond to the property of the system that a global radiative forcing of 1 Wm^{-2} (which results in an effective radiative forcing of 6 Wm^{-2} in the oceanic surface fraction) causes an increase of the average temperature of the system T_M of $\approx 0.6\ ^\circ C$ when equilibrium is re-established; this property can be summarized by introducing a climatic temperature/radiation *elasticity* parameter $\kappa_M \approx 0.6\ ^\circ C W^{-1} m^2$. Therefore, considering that it is estimated that in the real Earth system the doubling of CO_2 causes an average radiative forcing of $\approx 4\ Wm^{-2}$, we can loosely interpret the parameter κ_M as indicator of a *climate sensitivity* of $\approx 2.5\ ^\circ C$.

Substituting in 4.1 and 4.2 the equilibrium T_i of control run, we can derive the C_i such that we obtain $F_1 = 13.5 \cdot 10^{-11}\ s^{-1}$ and $F_3 = 9 \cdot 10^{-11}\ s^{-1}$. The latent heat fluxes are then obtained using equation 4.4, while the coefficients D_i for the sensible heat fluxes in 4.6 are derived by requiring that the total heat flux H_i in equation 4.3 of the coupled and of the uncoupled model match at the equilibrium solution. The relative magnitude of the latent and sensible heat fluxes LH_i and SH_i at equilibrium depend on the choice of $\gamma_1 = \gamma_3$ [Marotzke 1996]. We present in table A.2 the data relative to the values of the total surface heat flux and of the latent, sensible, and radiative heat components for the control run. While the sensible and latent heat fluxes into box 1 are roughly the same, in the case of box 3 the sensible heat flux is almost three times as large as the latent heat flux; the figures we obtain with our model are broadly in agreement with estimates [Peixoto and Oort 1992]. The parameter n determines the efficiency of the atmospheric transports in terms of its sensitivity to the meridional temperature gradient: we consider for n the values $[1, 3, 5]$, which include the domain proposed in [Held 1978] (2 to 5), but also include simple diffusive representation ($n = 1$).

4.3 Radiative forcings applied and feedbacks scheme of the system

In order to analyze the stability of the coupled model to radiative forcings, we increase the radiative equilibrium temperatures ϑ_i: such changes can be thought of as a natural representation of global warming scenarios. In the case of a coupled model, given that the fluxes depend both on averages and gradients of temperatures of neighboring boxes, changes in the parameter ϑ_2, which in the first approximation controls T_2, need to be considered in order to perform a complete and sensible study. As in the previous analysis, we alter the driving parameters ϑ_i by using a linear increase:

$$\vartheta_i(t) = \begin{cases} \vartheta_i(0) + \vartheta_i^t \cdot t, & 0 \leq t \leq t_0 \\ \vartheta_i(0) + \vartheta_i^t \cdot t_0. & t > t_0 \end{cases} \quad i = 1, 2, 3 \tag{4.9}$$

We make this choice because a linearly increasing radiative forcing approximately corresponds in physical terms to an exponential increase of the concentration of greenhouse gases [Shine et al. 1995, Stocker and Schmittner 1997]. The role of ϑ_2 is analyzed by considering three cases $\Delta\vartheta_2/\Delta\vartheta_1 = [1.0, 1.5, 2.0]$, where we have used the definition $\Delta\vartheta_i \equiv \vartheta_i^t \cdot t_0$. This allows for the fact that in global warming scenarios the net radiative forcing increase is larger in the tropics than in mid-high latitudes [Ramanathan et al. 1979], because of differences in the specific humidity. For a given choice of $\Delta\vartheta_2/\Delta\vartheta_1$, each forcing can be uniquely identified by the triplet $[t_0, \Delta\vartheta_3/\Delta\vartheta_1, \Delta\vartheta_1]$ and by the triplet $[t_0, \Delta\vartheta_3/\Delta\vartheta_1, \vartheta_1^t]$. Although only weakly asymmetric or symmetric forcings are representative of physically reasonable conditions, we consider general asymmetric forcings, in order to get a more complete picture of the mathematical properties of the system. We find that in most cases the destabilization of the THC occurs only if $\Delta\vartheta_1 \geq \Delta\vartheta_3$, therefore we perform the analysis of the feedbacks of the system - which are obviously coupled to the previously described oceanic feedbacks- under this condition. We observe that the first order effect of such a forcing is to weaken the THC, because the following relation holds:

- Increase in $\vartheta_2 \geq$ Increase in $\vartheta_1 \geq$ Increase in $\vartheta_3 \Rightarrow$ Increase in $H_2 \geq$ Increase in $H_1 \geq$ Increase in $H_3 \Rightarrow$ Increase in $T_2 \geq$ Increase in $T_1 \geq$ Increase in $T_3 \Rightarrow$ q decreases.

We underline that a larger radiative forcing in the tropical box decreases the stability of the circulation because it causes advection of warmer water from box 2 to box 1.

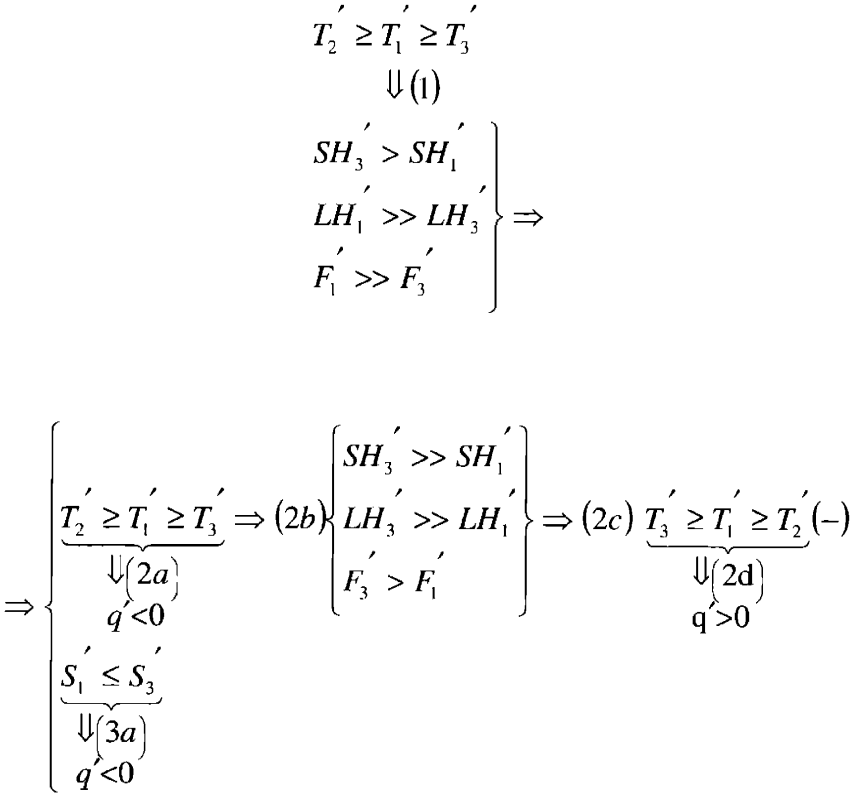

Figure 4-1: Atmospheric feedbacks scheme of the coupled model

The relative complexity of the coupled model makes the analysis of the feedbacks much more difficult than in the uncoupled model presented in chapter 2. In figure 4-1 we present a scheme describing the main atmospheric feedbacks; as previously noted in chapter 2, the symbol ' indicates that we are dealing with small perturbations from the equilibrium value of the variable which the prime symbol is referred to.

If T_2 increases more than T_1, which itself increases more than T_3, both the absolute value of the meridional temperature gradients and the average temperatures of box 1 and box 2, and of box 2 and box 3 increase, so that all the poleward atmospheric transports increase (step 1). The total effect is that box 1 heats up and freshens more than boxes 2 and 3 (step 2 and 3), so that the oceanic circulation weakens (steps $2a$ and $3a$). The strong increase of T_1 reduces $T_2 - T_1$ and so hinders the efficacy of the transport between these two boxes; this causes a great reduction of the freshwater flux and of the latent heat (and sensible heat) flux into box 1. On the contrary, for box 2 we obtain that the effect of the decrease of the meridional temperature gradient is relatively small and is compensated by the increase in the capacity of the atmosphere to retain moisture, so that the freshwater and total heat flux from box 2 to box 3

increase (step 2b). This causes a freshening and heating of box 3 relative to box 1 and box 2, so that the oceanic circulation is enhanced (step $2d$); we get temperature variations that are opposite to the initial variations, so that the thermic part of the total atmospheric feedback (step $2c$) is negative. Large values of n make the negative feedback in step $2b$ associated to the decrease of $T_2 - T_1$ more powerful; forcings with large $\Delta\vartheta_2$ can generally decrease the stability of the system because warmer tropical air can transport more freshwater and latent heat to the high-latitudes, and the effect is usually larger for the fluxes into box 1. Small values of $\Delta\vartheta_3/\Delta\vartheta_1$ will generate in steps $2a$ and $3a$ a very intense weakening of the THC and possibly its reversal. Therefore the whole process seems altogether dominated by the variations in the latent heat and freshwater fluxes.

4.4 Analysis of selected model runs

In figure 4-2 we show the time evolution of the THC strength q (we have chosen $n = 3$) for two different radiative forcings lasting 1000 years: the solid line describes the subcritical and the dashed line the supercritical case. In the subcritical case, the minimum value of THC strength (which is $\approx 6\ Sv$) is reached at $t \approx 450\ y$; after that, and so still within the phase of increasing forcing, q oscillates with a period of $\approx 400\ y$. This means that the negative feedbacks overcome the external forcing and stabilize the system. In the somewhat similar case shown in figure 2-6 for the uncoupled model the system closely followed the forcing up to the end of its increase; this relevant change in behavior of the system is essentially due to the conceptual difference between the target temperature restoring coefficient in the uncoupled model and the radiative temperature restoring coefficient B in the coupled model. We observe that at the newly established equilibrium -for $t \geq 1200\ y$- the THC strength is larger than before the perturbation, as observed in the uncoupled case for freshwater flux forcings presented in chapter 2; this means, considering that at equilibrium the value of q for a northern sinking equilibrium is given by equation 1.11, that the radiative forcing causes an increase in the southern Hemisphere poleward moisture flux F_3.

In order to explore the relevance of the sensitivity of the atmospheric transports in determining the intensity of the feedbacks of the system, we present in figures 4-3, 4-4, and 4-5 the effects for choices of $n = 1, 3, 5$ of a subcritical radiative forcing that lasts

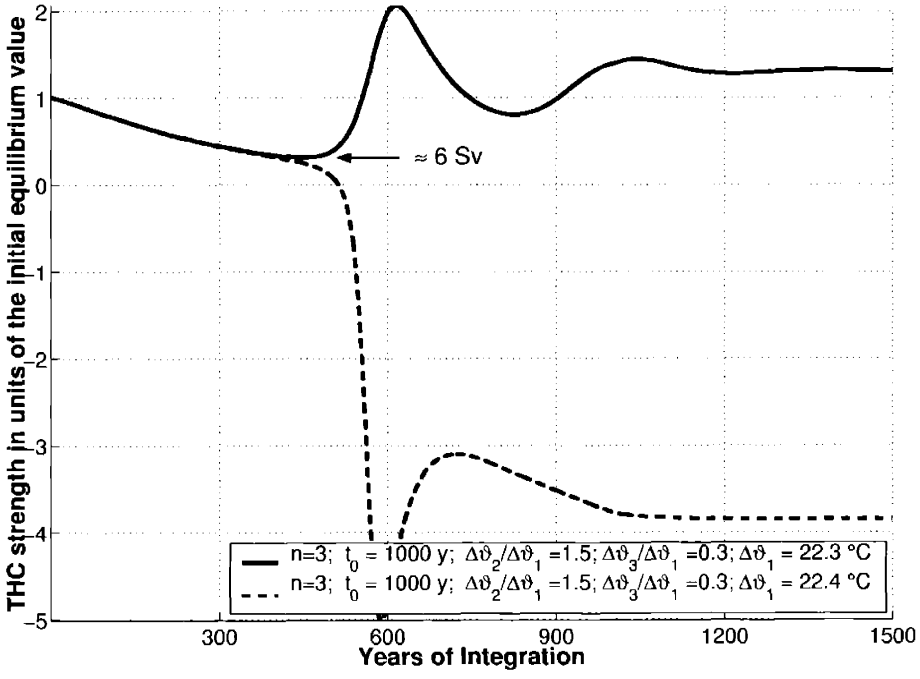

Figure 4-2: Evolution of the THC strength under a super- and sub-critical radiative flux forcing - Coupled Model

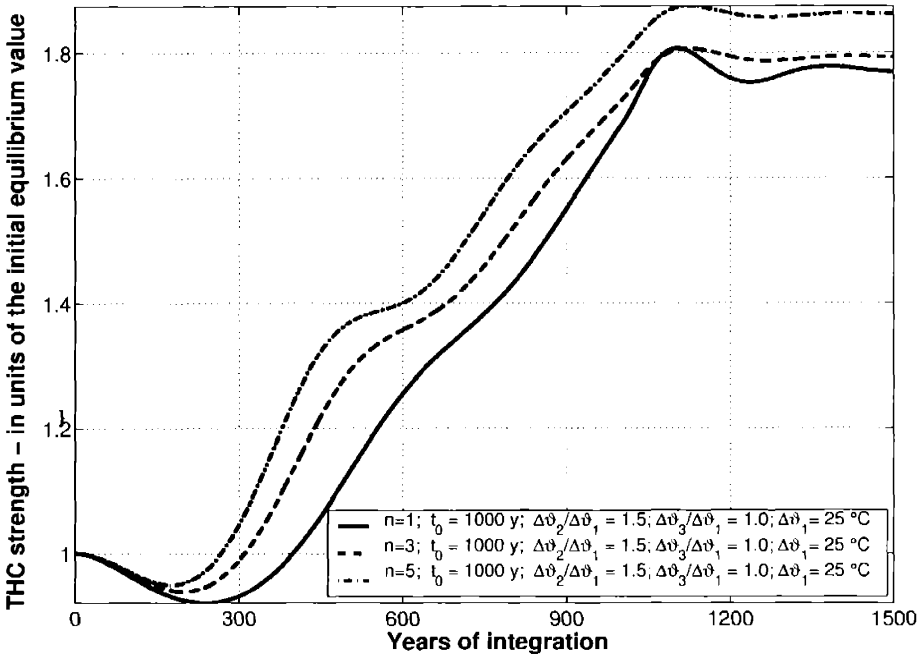

Figure 4-3: Influence of the atmospheric transport parametrization on the evolution of the THC strength for a given, non-destabilizing, radiative forcing - Coupled Model

1000 years and is such that the radiative equilibrium temperature increases by 2.5 $^{\circ}C$ per century in both the high-latitude boxes and by 3.75 $^{\circ}C$ per century in the tropical box; this corresponds to changes in the radiative forcings of $\approx 4\ Wm^{-2}$ per century and 6 Wm^{-2} per century respectively and so to a globally averaged increase of the radiative forcing of $\approx 5\ Wm^{-2}$ per century. In figure 4-3 we show the evolution of the THC circulation: in all the three cases the decline stops around 200-250 years after the beginning of the forcing, when the negative feedbacks of the system described in figure 4-1 become relevant. The robustness of having an initial THC decrease under global warming conditions, as discussed in [Tziperman 2000b], is then confirmed also for our model.

We see that the extent of the decline and its delay are negatively correlated with the value of the exponent for the atmospheric transport power law, thus suggesting that a more sensitive atmospheric transport is more effective in stabilizing the system.

In figure 4-4 we show that there is eventually a decrease of the meridional temperature gradients in both hemispheres; this means that the poleward heat transports must become so efficient that they overcome the larger radiative forcing in the tropics. Therefore, if we force the system more intensely at the tropics, the system response generally is not qualitatively different from what it is if the forcing is spatially constant.

Considering that the meridional temperature gradient is constant or decreases even when the THC slows down, and observing how small are the differences in the THC strength between $n = 1$ and $n = 5$ in figure 4-3 and how large are the differences in the meridional temperature gradients between $n = 1$ and $n = 5$ in figure 4-4, we can deduce that atmospheric heat transports' increased efficiency plays the major role in redistributing effectively the heat all over the globe ina global warming scenario. Considering that the evolution of the poleward latent heat transport in global warming scenarios is characterized by the competition between the increased capability of the atmosphere to retain moisture for higher average temperatures, due to the Clausius-Clapeyron relation, and the reduced efficiency in the atmospheric transport due to decreased meridional temperature gradient, as can be seen is equation 4.4, it is reasonable to guess that latent heat flux increases give the most relevant contribution to the increase in efficiency of the total atmospheric heat transport. Since the freshwater fluxes are proportional to the correpsonding latentheat fluxes, we have that they experience an analogously rich dynamics under global warming conditions,

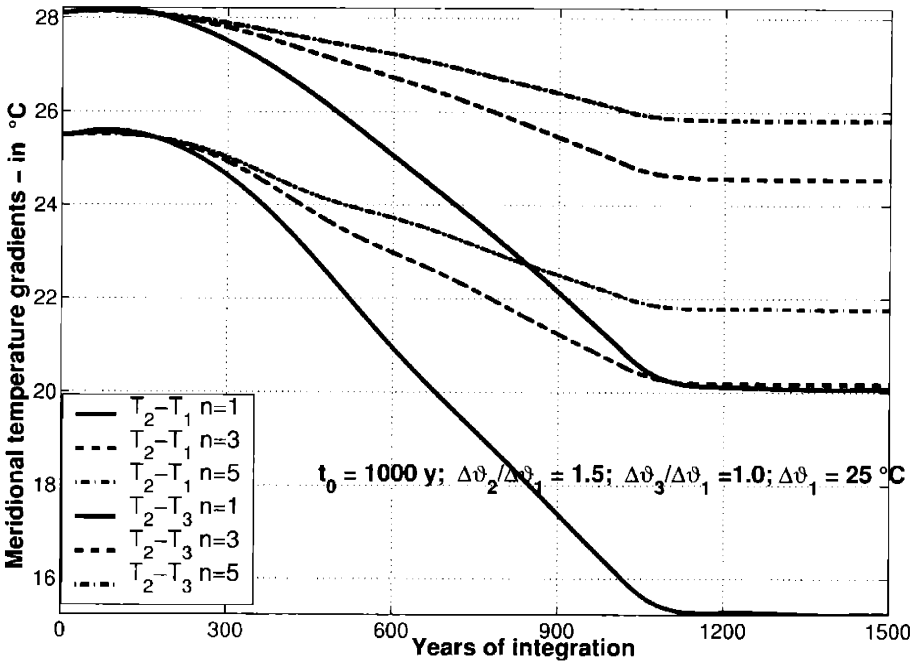

Figure 4-4: Influence of the atmospheric transport parametrization on the evolution of the Pole-to-Equator temperature gradients for a given, non-destabilizing, radiative forcing - Coupled Model

and it is reasonable to expect that freshwater fluxes's changes also paly a relevant role in both the destabilization and the stabilization of the THC. In the physical world, the effect described by the Clausius-Clapeyron equation actually dominates the freshwater and latent heat flux evolution for larger climate changes, as proved by positive correlation between average global temperature and accumulation in the glaciers in paleoclimatic data or simulations [Charles et al. 1994, Manabe and Stouffer 1994, Krinner and Genthon 1998, Kitoh et al. 2001], and it is reasonable to expect that similarly the Clausius-Clapeyron effect dominates the changes in the latent heat and freshwater fluxes in global warming scenarios[Tziperman and Gildor 2002].

4.4.1 Comparison between the relevance of latent heat vs. relevance of freshwater flux changes

In figure 4-5 we present in density units the contributions of the processes that tend to destabilize the THC: the change from the initial value (indicated by the symbol Δ) of the differences between the the freshwater fluxes, latent heat fluxes and total surface heat fluxes into box 1 and into box 3. We see that the contribution to the destabilization of the THC of the freshwater flux variation is quite small relatively

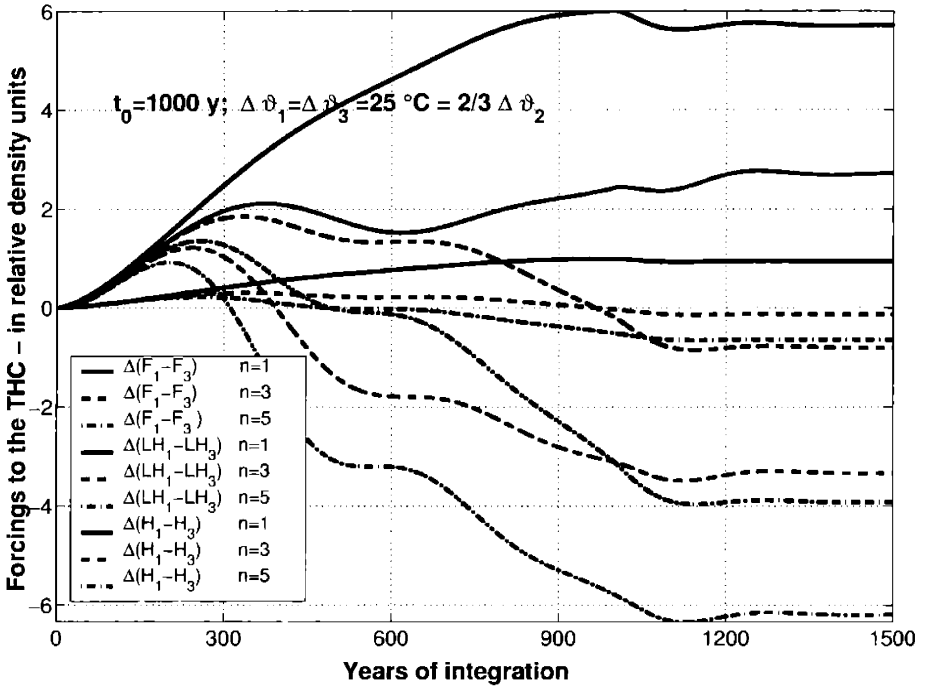

Figure 4-5: Influence of the atmospheric transport parametrization on the relative relevance of freshwater, latent heat and total atmospheric heat flux forcings for a given, non-destabilizing, radiative forcing - Coupled Model

to the contribution diue to the total heat flux; the main reason is that the increase of the latter is entirely due to the increase in the latent heat flux difference, which gives, as shown in equation 4.5, a contribution to the increase of buoyancy flux into box 1 that is about six times as large as the contribution due to the freshwater flux. The other components of the total heat flux tend to stabilize the system but their contribution in this sense is relatively negligible. Therefore the largest contribution to the destabilization is thermic and driven by the latent heat. This observation holds for all the three cases analyzed. In the longer term, when the THC recovers, the evolution of the total heat fluxes' difference between box 1 and box 3 changes notably with n, since it increases from the initial value for $n = 1$, while it decreases for $n = 3$ and $n = 5$. It is clear from the figures that most of this difference can be attributed to the difference of the latent heat fluxes between the two boxes 1 and 3 alone.

Two studies with coupled atmosphere-ocean GCMs have obtained contrasting results about the relative relevance of heat *vs.* freshwater as destabilizing mechanisms; in [Mikolajewicz and Voss 2000] it is shown that the heat flux change is the most important destabilizing mechanism and that this change is dominated by the latent heat flux, just as in our model. By contrast, in [Dixon et al. 1999] it is concluded

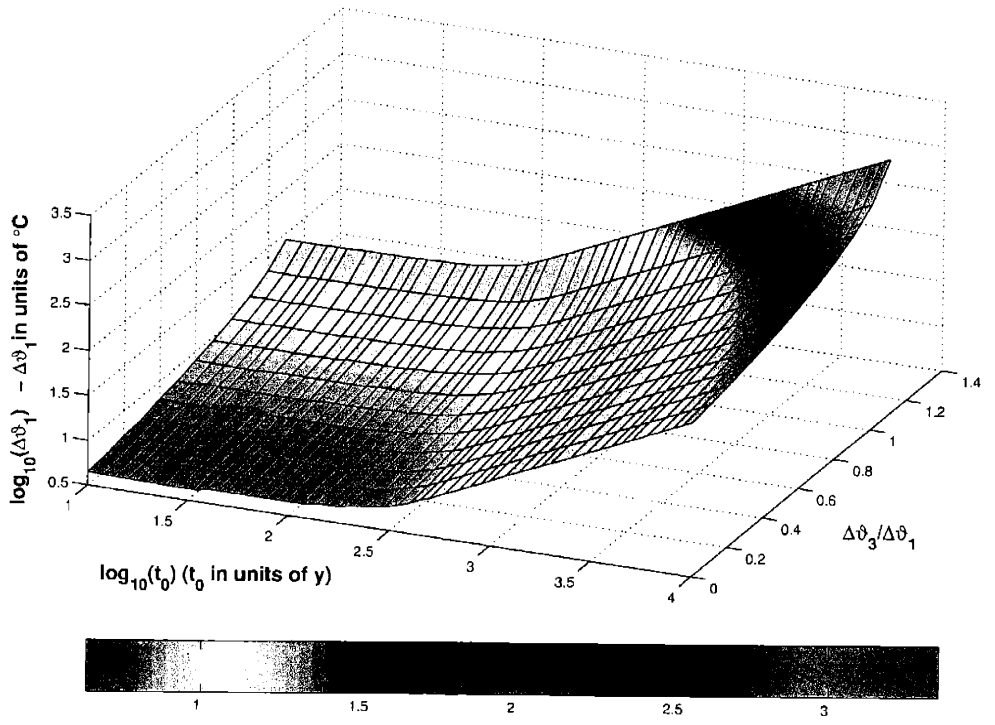

Figure 4-6: Critical values of the total increase of the radiative temperatures - Coupled Model

that changes in the moisture flux were the main destabilizing agent. However, calculations of the contributions of changes in both the heat and moisture fluxes to the change in the density flux in the model used in [Dixon et al. 1999] show that it is in fact dominated by the heat flux changes [Huang et al. 2003]. Indeed this is true of all the seven coupled GCMs analyzed in the context of the Climate Intercomparison Project (CMIP) [Huang et al. 2003]. This apparent contradiction may be explained by the results presented in [Kamenkovich 2003], where it is found that, even though the decrease in the thermohaline circulation may be initiated by changes in the moisture flux, changes in the heat flux induced by atmospheric feedbacks nevertheless contribuite strongly to the decrease.

4.5 Critical Perturbations

Once the parameters of atmospheric transport efficiency n and of ratio of the the box 2-to-box 1 radiative forcing are chosen, it is possible to uniquely identify each forcing applied using three coordinates, descriptive of the spatial and temporal pattern of the perturbation. In this section we present the set of critical forcings, which divide the

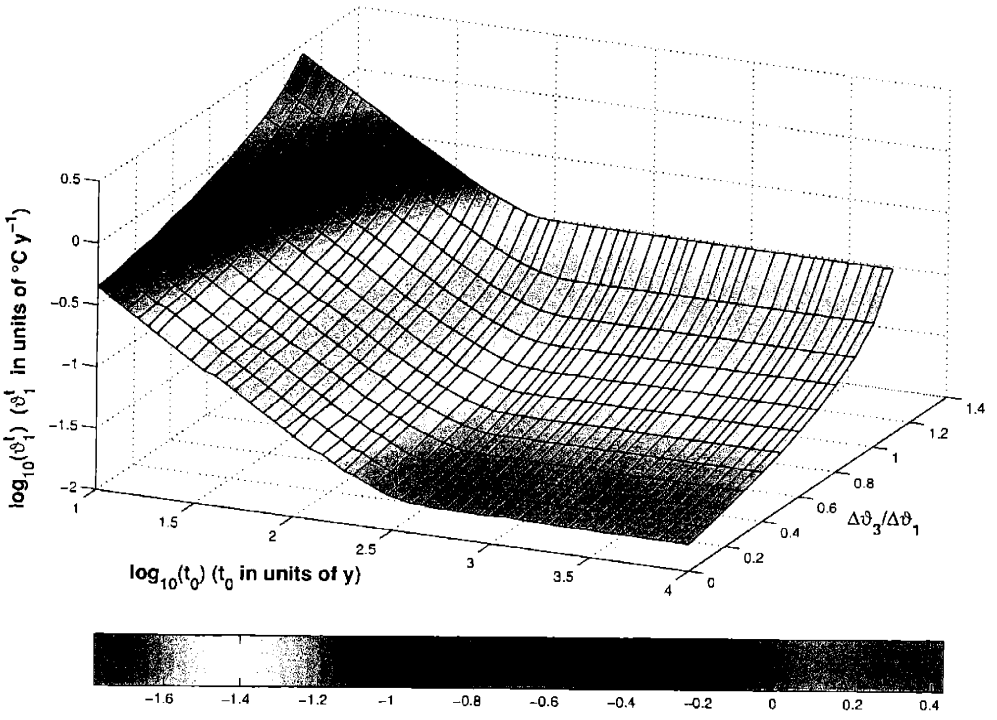

Figure 4-7: Critical values of the rate of increase of the radiative temperatures - Coupled Model

forcings that disrupt the present pattern of the THC from those that drive the system to a northern sinking state qualitatively similar to the initial unperturbed state. We consider an average *model+forcing* case, which is characterized by $n = 3$ and $\Delta\vartheta_2/\Delta\vartheta_1 = 1.5$. In figure 4-6 we present the manifold of those critical forcings using the coordinate system $[t_0, \Delta\vartheta_3/\Delta\vartheta_1, \Delta\vartheta_1]$, while in figure 4-7 we adopt the coordinate system $[t_0, \Delta\vartheta_3/\Delta\vartheta_1, \vartheta_1^t]$. There is a general agreement between the response of the coupled and of the uncoupled model to destabilizing perturbations. In figure 4-6 we observe that the more symmetric and the slower the forcing, the less likely is the destabilization of the THC:

- for a given $\Delta\vartheta_1$, the lower is the value of the ratio $\Delta\vartheta_3/\Delta\vartheta_1$, the lower is the total change $\Delta\vartheta_1$ needed to obtain the reversal of the THC;
- for a given value of the ratio $\Delta\vartheta_3/\Delta\vartheta_1$, more rapidly increasing perturbations (larger ϑ_1^t) are more effective in disrupting the circulation.

Nonetheless, the results for the coupled model differ from those obtained in the uncoupled case presented in chapter 2 for two main reasons, which are apparently con-

tradictory.

First, observing figure 4-6, we see that even for strongly asymmetric perturbations having very low values of $\Delta\vartheta_3/\Delta\vartheta_1$, there is a threshold in the rate of increase of the forcing below which the reversed THC does not occur, independently of the total radiative forcing realized; in figure 4-7 we can observe that, for each value of $\Delta\vartheta_3/\Delta\vartheta_1$, the critical value of the rate of increase of the forcing ϑ_1^t is independent of the temporal extension of the forcing t_0. This implies that for $n = 3$ the system cannot make transitions to a southern sinking equilibrium for quasi-static perturbations, since they would require indefinitely large perturbations. If $n = 1$ there is no threshold in the rate of increase for low values of $\Delta\vartheta_3/\Delta\vartheta_1$, which implies that in these cases quasi-static perturbations can cause the collapse of the THC; in order to explore this property of the system when the atmospheric transport is less sensitive to changes in the meridional temperature gradients, in section 4.7 we will discuss the bifurcation diagrams.

Second, we can obtain the collapse of the THC for forcings that are larger in the southern high latitude box (note that in figures 4-6 and 4-7 the domain extends beyond 1 in the $\Delta\vartheta_3/\Delta\vartheta_1$ direction). We can understand this behavior considering the feedback mechanism previously described in figure 4-2. In the first place, if $\Delta\vartheta_3 \geq \Delta\vartheta_1$, it is possible to obtain destabilization of the system in steps $2a$ and $3a$ if the forcing is fast (and so able to avoid the feedback steps $2b$ and $2c$), essentially because the equilibrium control of the latent heat and freshwater fluxes into box 1 is larger, and so a smaller relative increase can result is a larger absolute increase. Moreover, if the northern meridional temperature gradient is radiatively forced to increase more than the southern, the atmospheric diffusivity feedback will enhance more the sensible heat flux into box 1 in step 1. We note that in the uncoupled case it was not possible in any case to destabilize the THC if the forcings were stronger in box 3.

Previous studies focusing on more complex models obtain a similar dependence of thresholds on the rate of increase of the forcings [Stocker and Schmittner 1997, Schmittner and Stocker 1999], while in other studies where the full collapse of the THC is not obtained, it is nevertheless observed that the higher the rate of increase of the forcing, the larger the decrease of THC realized [Stouffer and Manabe 1999]. Other studies on coupled models also show how the spatial pattern of freshwater forcing due to global warming is extremely relevant especially in the short time scales:

only forcings occurring mainly in the northern Atlantic are efficient in destabilizing the THC [Rahmstorf 1996, Rahmstorf and Ganopolski 1999, Manabe and Stouffer 2000, Ganopolski et al. 2001].

4.6 Sensitivity Study

From the analysis of the figures 4-2, 4-3, 4-4, and 4-5 and from the analysis of the feedbacks of the system, we have found that the difference between the latent heat fluxes into the two high-latitude boxes dominates the dynamics of the forced system and determines its stability. Given the properties and the functional form of LH_1 and LH_3 we expect that:

1. the system is less stable against radiative forcings if the tropical to high latitudes radiation forcing ratio is larger, without preference for the time scale of the forcing;

2. in the case when the radiative forcing is larger in the northern high-latitude box than in the southern high-latitude box, the system is more stable if the atmospheric transport feedback is stronger; this effect is likely to be notable *only if* the perturbations have times scales larger than the flushing time of the oceanic boxes, as confirmed in the extreme case of quasi-static perturbations;

3. in the case when the radiative forcing is fast and larger in the southern high-latitude box than in the northern high-latitude box, the system is less stable if the atmospheric transport feedback is stronger.

To obtain a more quantitative measure of which processes are important, we analyze the sensitivity of the $z-$coordinate of the the manifold of the critical perturbations shown in figure 4-6 to changes in key parameters; we define Z_C as the the critical values of $\Delta\vartheta_1$ presented in figure 4-6. In particular we consider the 2-dimensional fields of the finite difference estimates of the partial derivatives $\partial(Z_C)/\partial(\Delta\vartheta_2/\Delta\vartheta_1)$ and $\partial(Z_C)/\partial(n)$. Figure 4-8 shows $-\partial(Z_C)/\partial(\Delta\vartheta_2/\Delta\vartheta_1)$. This manifold is very similar to figure 4-6: this suggests that Z_C changes roughly in proportion to its actual value when $\Delta\vartheta_2/\Delta\vartheta_1$ changes. In figure 4-9 we present the manifold given by the values of $-\partial(Z_C)/\partial(\Delta\vartheta_2/\Delta\vartheta_1)\cdot 1/(Z_C)$. This manifold is effectively flat for $\Delta\vartheta_3/\Delta\vartheta_1 \leq 0.7$ and is everywhere independent of the value of t_0. In physical terms, this means that the increase in the ratio between the tropical and the northern high latitudes

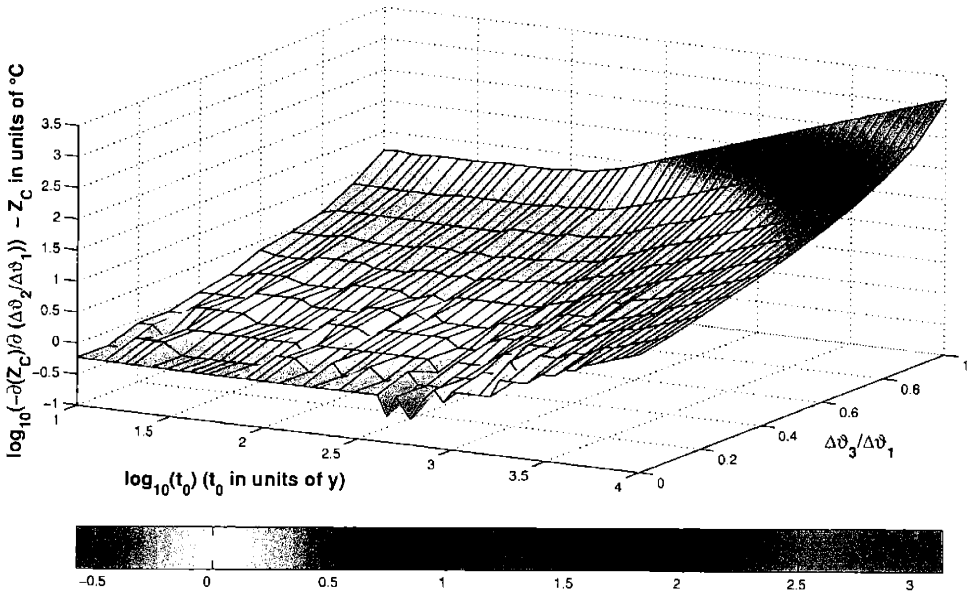

Figure 4-8: Sensitivity to the low-to-high latitudes radiative forcing ratio of of the critical values of the total increase of the radiative temperatures - Coupled Model

radiative forcing changes the response of the system and favors the collapse of the THC evenly and independently of the temporal scale of the forcing itself, and is particularly effective if we use quasi-symmetric forcings. Therefore the change of the parameter $\Delta\vartheta_2/\Delta\vartheta_1$ does not have preferential effect on any of the feedbacks. Figure 4-10 presents the value of $\partial(Z_C)/\partial(n)$. We observe that this graph has almost no $\Delta\vartheta_3/\Delta\vartheta_1$ dependence, and its most striking feature is that the surface rises abruptly from a flat and low region for $t_0 \approx 300\ y$. The sensitivity of the measure of the system stability to the radiative forcings with respect to the efficiency of the atmospheric transport feedback is small and positive for forcings having temporal scale shorter than the characteristic oceanic time scale of the system, while it becomes very large and positive for forcings having long temporal scales. The positive value means that a more sensitive atmospheric transport (higher values of n) stabilizes if $\Delta\vartheta_3/\Delta\vartheta_1 \leq 1$. With a more temperature-gradient sensitive atmospheric transport smaller changes in temperature gradients between the boxes are needed (see figure 4-4) to change *all* the atmospheric fluxes; therefore the system is able to dynamically arrange very effectively the atmospheric fluxes, so that they can counteract more efficiently the external forcings and keep the system as close as possible to the initial state. If the forcings are very fast, the enhancement of the atmospheric stabilizing mechanism is not very effective. On the contrary, for slow forcings in-

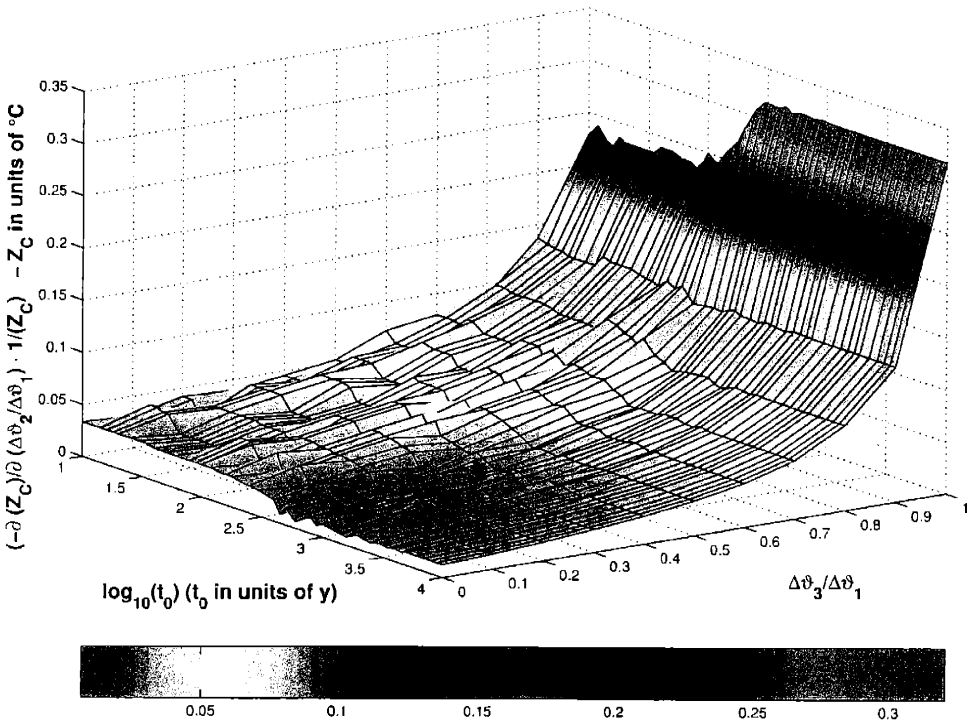

Figure 4-9: Weighted sensitivity to the low-to-high latitudes radiative forcing ratio of of the critical values of the total increase of the radiative temperatures - Coupled Model

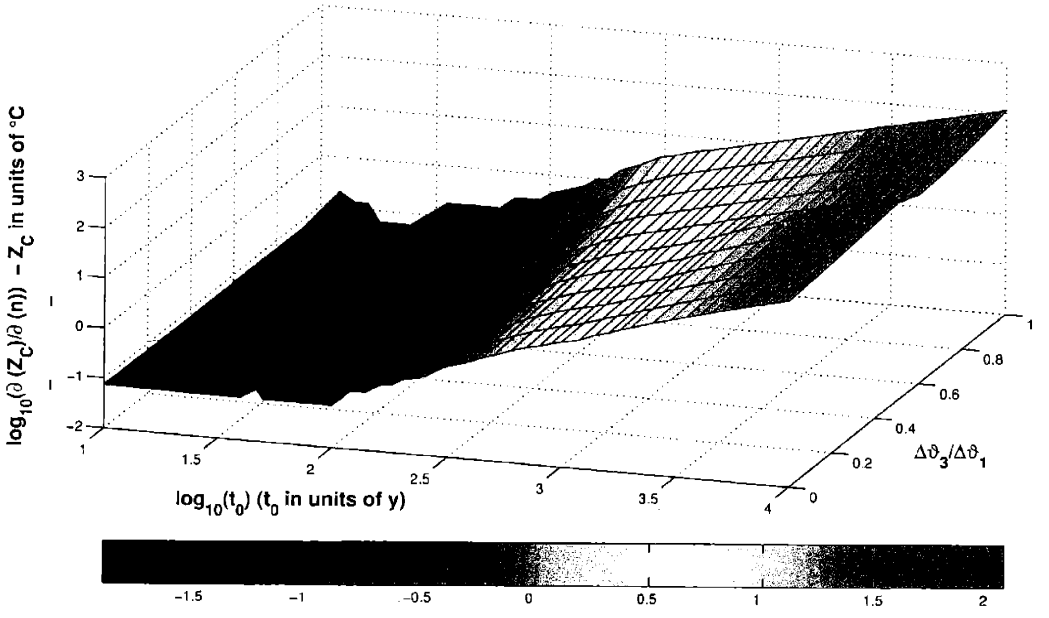

Figure 4-10: Sensitivity to the atmospheric transport parametrization of of the critical values of the total increase of the radiative temperatures - Coupled Model

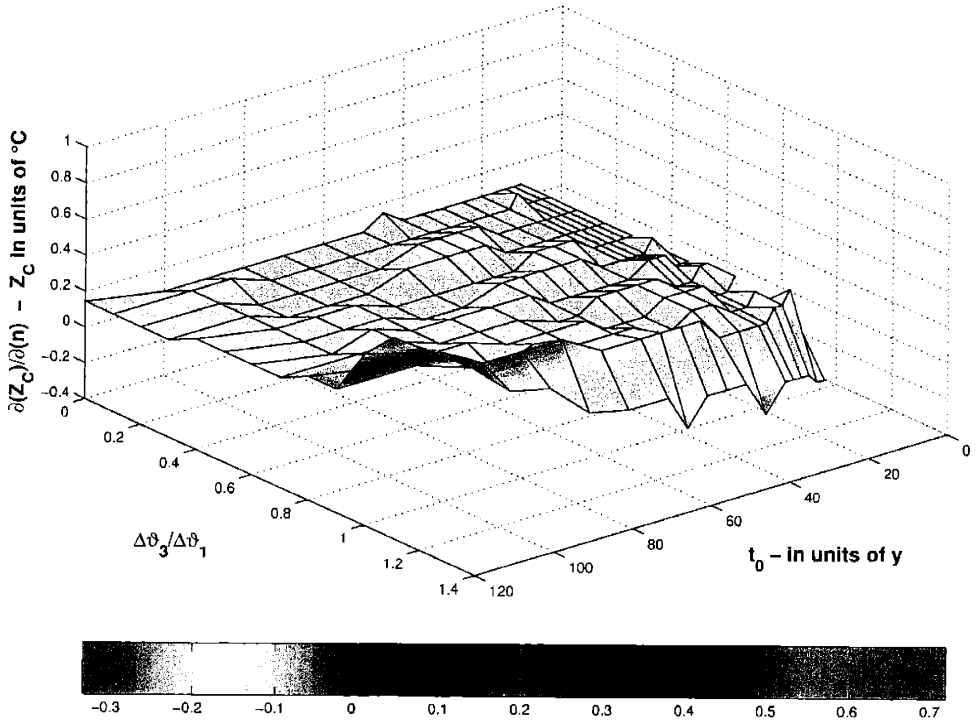

Figure 4-11: Sensitivity to the atmospheric transport parametrization of of the critical values of the total increase of the radiative temperatures (detail) - Coupled Model

volving time scales comparable to or larger than those of the system, the enhanced strength of the negative feedback obtained with increasing efficiency of the atmospheric transport can play a very significant stabilizing role in the dynamics of the system. This seem to be in contrast with the result that in the uncoupled model shorter relaxation times for box temperatures -which as shown in [Marotzke 1996] correspond to more sensitive atmospheric heat transports- imply less stability for the system [Tziperman et al. 1994, Nakamura et al. 1994, Rahmstorf 2000]. Actually the contrast is only apparent, the point being that in an uncoupled model there is no adjustment of of moisture fluxes due to temperature changes: therefore decreasing the relaxation time make the system *less flexible* and adaptable to forcings. Our results seem to disagree with the conclusions drawn in the coupled model presented in [Scott et al. 1999]. We think that the disagreement is mainly due to the fact that in this study we are dealing with a different kind of perturbation, descriptive of global warming, and that these perturbations have a direct and strong influence on the most relevant atmospheric fluxes, because of their highly nonlinear dependence on average temperature changes; this property was not present in the parametrizations used in

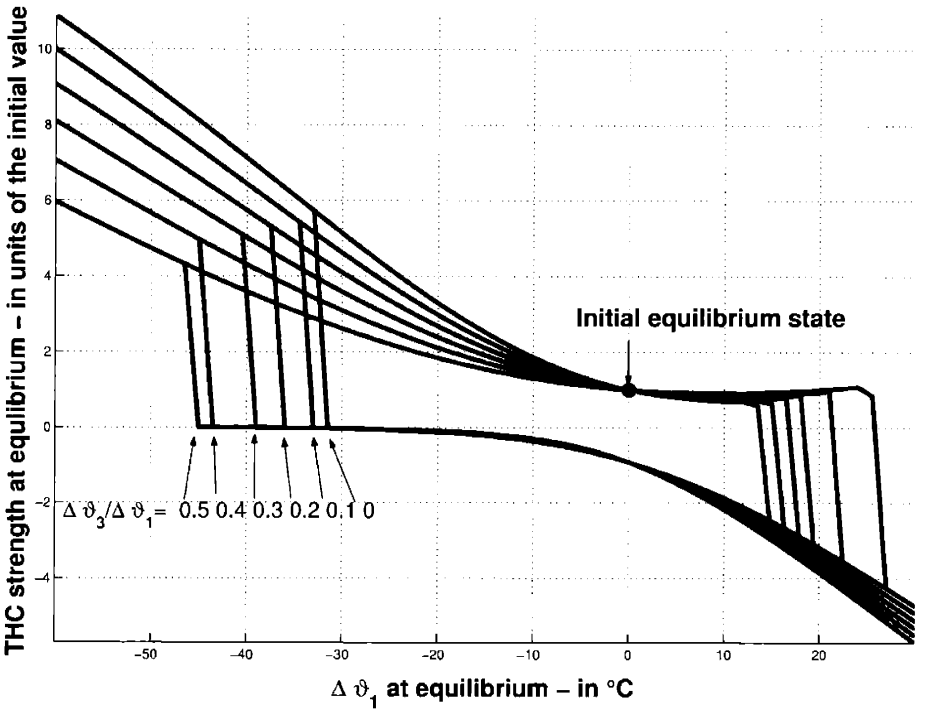

Figure 4-12: Bifurcation diagram of radiative temperature perturbations - Coupled Model with $n = 1$

[Scott et al. 1999].

By contrast with the above described result, we see in figure 4-11 that for $\Delta\vartheta_3/\Delta\vartheta_1 > 1$ and $t_0 \leq 80\ y$, the sensitivity $\partial(Z_C)/\partial(n)$ is negative, therefore a system with larger n is more easily destabilized. The destabilizing feedbacks in the special case $\Delta\vartheta_3/\Delta\vartheta_1 > 1$ discussed in the previous section become more and more relevant with increasing n: this is especially clear for the increase of efficiency of the destabilizing changes in sensible heat for higher power laws for the diffusivity.

4.7 Bifurcations

Choosing quasi-static perturbations to the radiative temperatures can lead to the reversal of the THC only if we select $n = 1$; this qualitative difference between the behavior of the various versions of the model is independent of the parameter $\Delta\vartheta_2/\Delta\vartheta_1$, because with a more temperature-gradient sensitive atmospheric transport the system is always able to counteract a slowly increasing destabilizing radiative forcing. With the choice of $n = 1$ and $\Delta\vartheta_2/\Delta\vartheta_1 = 1.5$, we have that quasi/static perturbations are destabilizing only if $\Delta\vartheta_3/\Delta\vartheta_1 \leq 0.5$. We present in figure 4-12 the

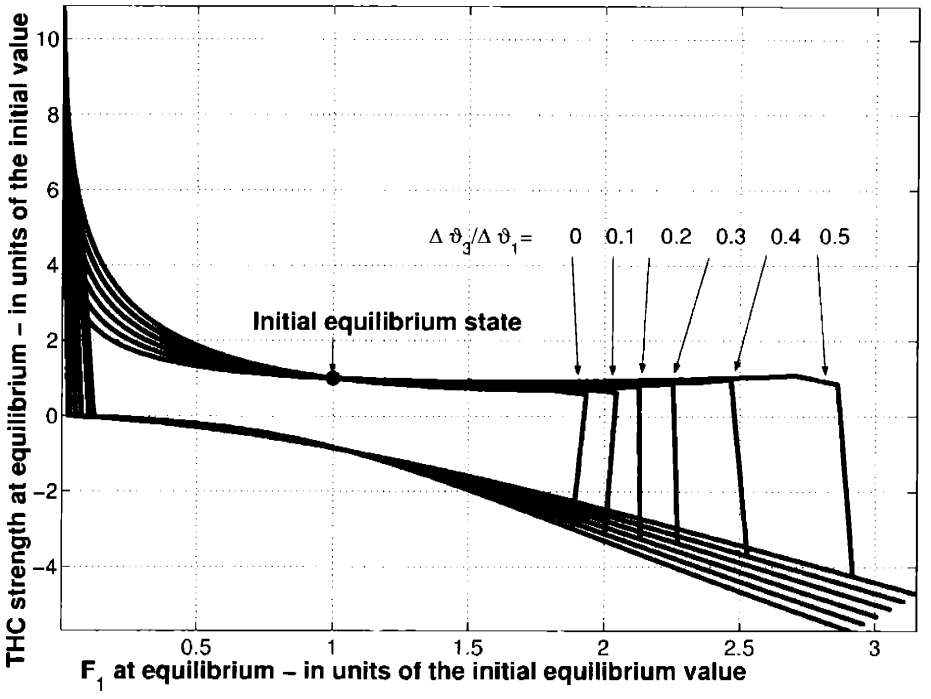

Figure 4-13: Bifurcation diagram of freshwater flux perturbations - Coupled Model with $n = 1$

bifurcation diagrams relative to $\Delta\vartheta_3/\Delta\vartheta_1 = [0, 0.1, 0.2, 0.3, 0.4, 0.5]$; we have $\Delta\vartheta_1$ as abscissa and q in units of the initial equilibrium value as ordinate, so that the initial state is the point $(0, 1)$. The abscissae of the subcritical Hopf bifurcation points on the right hand-side of the graph increase with increasing value of $\Delta\vartheta_3/\Delta\vartheta_1$ from $\approx 12°C$ to $\approx 25°C$, while the ordinates are close to 1, thus implying that when the bifurcation occurs the the THC is only slightly different from the initial equilibrium value. The bistable region is remarkably large in all cases, the total extent increasing with increasing value of $\Delta\vartheta_3/\Delta\vartheta_1$, because the abscissae of the bifurcation points in the left hand-side of the graph circuits are in all cases below $-30°C$ and so well within the unphysical region of parameter space. This means that once the circulation has reversed, the newly established pattern is extremely stable and can hardly be changed again. In figure 4-13 we present a bifurcation graph where the abscissa is the value of the freshwater flux into box 1 when the radiatively forced system has reached a newly established equilibrium (the initial equilibrium is the point (1,1)): we can see that there is a monotonic 1 to 1 mapping between figures 4-12 and 4-13 (apart from a very limited region around the bifurcation point in the right hand side for low $\Delta\vartheta_3/\Delta\vartheta_1$ values), which suggests that in our model, for a given value of $\Delta\vartheta_3/\Delta\vartheta_1$, at equilibrium the changes of the average surface temperature and the changes in the

intensity of the hydrological cycle are positively correlated. We observe that in terms of freshwater flux the bistable region is very limited (almost by an order of magnitude) with respect to the uncoupled case (see figure 2-5), thus suggesting a caveat in the interpretation of uncoupled models' results.

Chapter 5

Conclusions

5.1 Analysis of the results

In this dissertation we have analyzed the stability of the THC as described by two uncoupled models, differing for the choice of the boundary conditions, and a set of coupled models differing in the ratio between the radiative forcing realized at the tropics and at high latitudes and in the parametrization of the atmospheric transports.

The main results obtained with the uncoupled model with mixed BCs and presented in chapter 2 have been reported in [Lucarini and Stone 2003a], while the main results obtained with the coupled model and presented in chapter 4 have ben reported in [Lucarini and Stone 2003b]; most of the results of the thesis have been collected in [Lucarini and Stone 2003c].

In the case of the uncoupled model, we simulate the radiative forcing by applying to the equilibrium state perturbations to the moisture and heat fluxes into the three boxes. High rates of increase in the moisture flux into the northern high-latitude box lead to a THC breakdown at smaller final increases than low rates, while the presence of moisture flux increases into the southern high-latitude box strongly inhibit the breakdown. Similarly, fast heat flux increases in the North Hemisphere destabilize the system more effectively than slow ones, and again the enhancement of the heat fluxes in the southern Hemisphere tend to drive the system towards stability. In particular the relevance of the role of changes in the freshwater flux into the southern ocean is determined, along the lines of [Scott et al. 1999] for a similar box model and [Wang et al. 1999a] for an OGCM. In all cases analyzed slow forcings, if asymmetric enough, lead to the reversal of the THC. We conclude that the study of the THC system change under perturbations with uncoupled models, of any level of complexity, should take into much greater account the spatial (see [Rahmstorf 1995, Rahmstorf 1996]) and temporal pattern of forcings, in order to explore the full nonlinearity and the very different time-scales of the system. We have also presented bifurcations diagrams for freshwater fluxes perturbations that reproduce and extend the results previously given in the literature, because the effect of freshwater flux increases in the southern ocean are included, while for the first time bifurcation diagrams for heat flux forcings, obtained by perturbation of the target temperature, are presented.

In the coupled model a more natural representation of the radiative forcing is possible, since the main atmospheric physical processes responsible for freshwater and heat fluxes are formulated separately. Although only weakly asymmetric or symmet-

ric radiative forcings are representative of physically reasonable conditions, we have considered general asymmetric forcings, in order to get a more complete picture of the mathematical properties of the system. We have analyzed five combinations of the system *model+radiative forcing*, considering different combinations of the atmospheric transport parametrization and of the ratio between the high to low latitudes radiative forcing. We generally find that fast forcings are more effective than slow forcings in disrupting the present THC patterns, forcings that are stronger on the northern box are also more effective in destabilizing the system, and that very slow forcings do not destabilize the system whatever their asymmetry, unless the atmospheric transport is only weakly dependent on the meridional temperature gradient. When the system is radiatively forced, initially the latent heat fluxes and the freshwater fluxes are strongly enhanced, thanks to the increase in the saturation pressure of the water vapor due to the warming, and the fluxes into the northern high latitude box increase. These are the main causes for the reduction of the THC strength. The strong increase of heat flux into box 1 reduces the efficacy of the atmospheric transport and so causes a great reduction of the freshwater flux and of the latent heat (and sensible heat) flux into box 1, which induces an increase in the THC. The variations of latent heat fluxes and of freshwater fluxes into the two high-latitude boxes, or better, the difference between the variations of those fluxes in box 1 and box 3, then dominate the dynamics of the forced coupled model, the main reason being, in the context of global warming experiments, the very strong dependence of these fluxes on the average temperature due to the Clausius-Clapeyron relation. In particular, in our system the major role is played by the latent heat because in density terms it is stronger than the freshwater flux by a factor of ≈ 6. A qualitatively similar dominance is found by some authors [Mikolajewicz and Voss 2000], and especially in the CMIP models [Huang et al. 2003], while other studies suggest that it is the freshwater flux to be dominant [Stocker and Schmittner 1997, Rahmstorf and Ganopolski 1999, Schmittner and Stocker 1999, Manabe and Stouffer 1999b, Ganopolski et al. 2001].

The inclusion of this relation in the fluxes' parametrization seem to play a key role in all the results obtained in our study. A sensitivity study performed on the ratio between the tropical and the high-latitudes radiative forcing and on the parametrization of the atmospheric transport supports the conclusion that including the Clausius-Clapeyron relation in the fluxes' parametrization plays a key role in all the results obtained in our study. We underline that the sensitivity study here proposed could

represent a good methodology to define more quantitatively the relative importance of the feedback mechanisms acting on the system when it is driven out of equilibrium.

Our work especially underlines how dramatic is the relevance of the considering different temporal patterns of forcings in order to realistically assess the response of the THC in global warming scenarios, because the THC dynamics encompasses very different time-scales, which can be explored only if the timings of the forcings are varied. Our results confirm what obtained by [Tziperman and Gildor 2002] for a hemispheric coupled box model and confirm the results obtained by [Stocker and Schmittner 1997, Schmittner and Stocker 1999] in the context of EMICSs and by [Manabe and Stouffer 1999a, Manabe and Stouffer 1999b, Manabe and Stouffer 2000, Stouffer and Manabe 1999] in the context of GCMs, thus completing the whole hierarchical ladder of model and providing evidence for the robustness of these results. Therefore the effect of changing the rate of increase of the radiative forcing should be explored in great detail with complex models, thus providing a bridge between the results obtained with the two most commonly considered scenarios, i.e. instantaneous and quasi-static pertubations.

We also underline that, since the THC is a highly nonlinear and nonsymmetric system, very relevant information on its dynamics could be gathered by analyzing with more complex climate models the dependence of the THC response on the spatial pattern of the effective radiative forcing realized in global warming scenarios.

5.2 Improvements and further study

We conclude by pointing out some possible improvements to the present model and possible extensions of this work.

In this study we have put emphasis on how the atmospheric transport processes, the local radiative budget and the oceanic advection can reverse the symmetry of the pattern of the circulation in the context of a rigorously symmetric geometry. The system is likely to be very sensitive to changes in the volumes of the boxes and especially to the introduction of asymmetries between the two high-latitude boxes, which would also make the system more realistic since the the southern mid-high latitude portion of the Atlantic is considerably larger than the northern mid-high latitude portion. Asymmetries in the oceanic fractional areas would induce asymmetries in the values of λ_i and B_i, thus causing the presence of different restoring times for the various

boxes, while asymmetries in the freshwater catchment areas ($\gamma_1 \neq \gamma_3$) would make the relative importance of the latent heat fluxes and of the freshwater fluxes (when expressed in common density units) different in the two boxes $i = 1, 3$.

The debated question of whether the heat or freshwater fluxes are the most relevant in destabilizing the THC circulation would benefit of including a more appropriate nonlinear equation of state for the water density; the likely effect would be increasing the relevance of the freshwater fluxes.

The presence of the albedo feedback would also introduce asymmetry between the two high latitudes boxes: it could be included in the model by parameterizing the radiative terms A_i as increasing functions of the temperatures T_i, along the lines of [Stocker and Schmittner 1997, Schmittner and Stocker 1999, Tziperman and Gildor 2002], considering the temperatures as proxies for the fraction of the surface covered by ice; we expect that the inclusion of an ice-albedo feedback would decrease the stability of the THC. Another positive feedback could be implemented in the model by considering the role of the THC in buffering the CO_2 changes by favoring ocean uptake; the model could be improved by prescribing a dependence of the radiative forcing on the strength of the THC.

In order to include a more realistic perspective of the energetics of the THC, it could be interesting to implement a functional dependence of the THC on the winds; an idea could be teh introduction of a variable hydraulic constant k depending on, e.g., the northern meridional temperature gradient, which is strictly related to intensity of the zonal winds.

Adding a noise component in the tendency equations [Titz et al. 2002a, Titz et al. 2002b], i.e. making the evolution of the system not deterministic, would increase the model's realism and make the model conceptually more satisfying; recent studies have undertaken this strategy and shown that close to instability threshold the evolution of the THC has a very limited predictability [Wang et al. 1999a, Knutti and Stocker 2002], and that stochastic resonance could be responsible for glacial/interglacial climate shift [Ganopolski and Rahmstorf 2002]. It would be interesting to analyze how the intensity and the color of the noise would influence the results obtained and the conclusions drawn in this work.

Another improvement to the model could be the addition of boxes descriptive of other oceanic basins, in order to represent the main features of the whole conveyor belt, along the lines of some examples presented in [Weaver and Hughes 1992].

Appendix A

Tables

Quantity	Symbol	Value
Mass of Box $i = 1, 3$	M	$1.08 \cdot 10^{20}\ Kg$
Box2/Box$i = 1, 3$ mass ratio	V	2
Average water density	ρ_0	$1000\ Kg\ m^{-3}$
Specific heat per unit mass of water	c_p	$4 \cdot 10^3\ J\ °C^{-1} Kg^{-1}$
Latent heat per unit mass of water	L_v	$2.5 \cdot 10^6\ JKg^{-1}$
Gas constant	R_v	$461\ J\ °C^{-1} Kg^{-1}$
Average Salinity	S_0	$35\ psu$
Oceanic fractional area	ϵ	1/6
Box $i = 1, 3$ fractional water catchment area	$1/\gamma_i$	1/2
Thermal expansion coefficient	α	$1.5 \cdot 10^{-4}\ °C^{-1}$
Haline expansion coefficient	β	$8 \cdot 10^{-4}\ psu^{-1}$
Hydraulic constant	k	$1.5 \cdot 10^{-6}\ s^{-1}$
Atmospheric temperature restoring coefficient[a]	$\tilde{\lambda}$	$25.8\ Wm^{-2}\ °C^{-1}$
Global climatic temperature/radiation elasticity [b]	κ_M	$0.6\ °C\ W^{-1} m^2$

Table A.1: Value of the main model constants

[a]Uncoupled Model - Value relative to the oceanic surface fraction only

[b]Coupled model - Value relative to the whole planetary surface; corresponds to a *Global climate sensitivity* per CO_2 doubling of $\approx 2.5\ °C$

Constant	Units	Box 1	Box 2	Box 3
Temperature	$^{\circ}C$	2.9	28.4	0.3
Salinity	psu	34.7	35.6	34.1
Atmospheric Freshwater Flux	Sv	0.41	-0.68	0.27
Total Surface Heat Flux	PW	-1.58	1.74	-0.16
-Latent Heat Flux[a]	PW	1.84	-3.06	1.22
-Sensible Heat Flux[a]	PW	2.14	-5.75	3.61
-Radiative Heat Flux[a]	PW	-5.57	10.57	-5.00
Oceanic Heat Flux	PW	1.58	-1.74	0.16
THC strength	Sv	15.5	15.5	15.5
Target Temperature[b]	$^{\circ}C$	0	30	0
Radiative Equilibrium Temperature[a]	$^{\circ}C$	-22.9	52.9	-22.9

Table A.2: Value of the fundamental parameters of the system at the initial equilibrium state

[a]Coupled Model
[b]Uncoupled Model

Bibliography

[Adkins et al. 1998] Adkins, J.F., H. Cheng, E.A. Boyle, E.R.M. Duffel, R.L. Edwards, Deep-sea coral evidence for rapid change in ventilation of the Deep North Atlantic 15400 years ago, Science 280, 725-728 (1998)

[Baumgartner and Reichel 1975] Baumgartner A., and E. Reichel, The World Water Balance (Elsevier, New York, 1975)

[Blunier et al. 1997] Blunier, T., J. Schwander, B. Stauffer, T. Stocker, A. Duellenbach, J. Indermuehle, J. Tschumi, D. Chappellaz, D. Raynaud, and J.-M. Barnola, Timing of the Antarctic Cold Reversal and the atmospheric CO2 increase with respect to the Younger Dryas event., Geophys. Res. Lett. 24, 2683-2686 (1997)

[Blunier et al. 1998] Blunier, T., J. Chappellaz, J. Schwander, A. Duelenbach, B. Stauffer, T. F. Stocker, D. Raynaud, J. Jouzel, H. B. Clausen, C. U. Hammer, S. J. Johnsen, Asynchrony of Antarctic and Greenland climate during the last glacial. Nature 394, 739-743 (1998)

[Boyle and Keigwin 1987] Boyle E. A., and L. Keigwin, North Atlantic thermohaline circulation during the past 20000 years linked to high-latitude surface temperature, Nature 330, 35-40 (1987)

[Bretherton 1982] Bretherton F. P., Ocean climate modeling, Progr. Oceanogr., 11, 93-129 (1982)

[Broecker 1991] Broecker W.S., The great ocean conveyor, Oceanography 4, 79-89 (1991)

[Broecker 1994] Broecker, W. S., Massive iceberg discharges as triggers for global climate change, Nature 372, 421-424 (1994)

[Broecker 1997] Broecker W. S., Thermohaline circulation, the Achilles heel of our climate system: Will man-made CO2 upset the current balance? Science, 278, 1582-1588 (1997)

[Broecker et al. 1985] Broecker W. S., D. M. Peteet, and D. Rind, Does the ocean-atmosphere system have more than one stable mode of operation?, Nature, 315, 21-26 (1985)

[Bryan 1986] Bryan, F., High-latitude salinity effects and interhemispheric thermohaline circulations, Nature, 323, 301-304 (1986)

[Charles et al. 1994] Charles, C. D., D. Rind, J. Jouzel, R. D. Koster, and R. G. Fairbanks, Glacial/interglacial changes in moisture sources for Greenland: Influences on the ice core record of climate, Science, 263, 508-518 (1994)

[Cubasch et al. 2001] Cubasch, U., G. A. Meehl, G. J. Boer, R. J. Stouffer, M. Dix, A. Noda, C. A. Senior, S. Raper, K. S. Yap, A. Abe-Ouchi, S. Brinkop, M. Claussen, M. Collins, J. Evans, I. Fischer-Bruns, G. Flato, J. C. Fyfe, A. Ganopolski, J. M. Gregory, Z.-Z. Hu, F. Joos, T. Knutson, R. Knutti, C. Landsea, L. Mearns, C. Milly, J. F. B. Mitchell, T. Nozawa, H. Paeth, J. Risnen, R. Sausen, S. Smith, T. Stocker, A.Timmermann, U. Ulbrich, A. Weaver, J. Wegner, P. Whetton, T. Wigley, M. Winton, and F. Zwiers, 9. Projections of future climate change, pp. 526-582 in "Climate Change 2001: The Scientific Basis. Contribution of Working Group I to the Third Assessment Report of the Intergovernmental Panel on Climate Change" (Cambridge University Press, Cambridge, 2001)

[Dixon et al. 1999] K. W. Dixon, T. L. Delworth, M. J. Spelman, and R. J. Stouffer, The influence of transient surface fluxes on North Atlantic overturning in a coupled GCM climate change experiment, Geophys. Res. Lett. 26, 2749-2752 (1999)

[Gill 1982] Gill A.E., Atmosphere-Ocean Dynamics (Academic Press, London, 1982)

[Ganopolski and Rahmstorf 2001a] Ganopolski, A. and S. Rahmstorf, 2001, Simulation of rapid glacial climate changes in a coupled climate model. Nature, 409, 153-158 (2001)

[Ganopolski and Rahmstorf 2001b] Ganopolski, A. and S. Rahmstorf, Stability and variability of the thermohaline circulation in the past and future: a study with a coupled model of intermediate complexity, pp. 261-275 in The Oceans and Rapid Climate Change: Past, Present and Future, D. Seidov, M. Maslin and B. J. Haupt Eds., (AGU, Washington, 2001)

[Ganopolski and Rahmstorf 2002] Ganopolski, A. and S. Rahmstorf, Abrupt Glacial Climate Changes due to Stohastic Resonance, Phys. Rev. Lett. 88, DOI 038051 (2002)

[Ganopolski et al. 2001] Ganopolski, A., V. Petoukhov, S. Rahmstorf, V. Brovkin, M. Claussen and C. Kubatzki, 2001: CLIMBER-2: A climate system model of intermediate complexity. Part II: Model sensitivity. Clim. Dyn. 17, 735-751 (2001)

[Held 1978] Held, I.M., The vertical scale of an unstable baroclinic wave and its importance for eddy heat flux parameterizations, J. Atmos. Sci. 35, 572-576 (1978)

[Huang et al. 2003] Huang B., P. H. Stone, A. P. Sokolov, and I. V. Kamenkovich, 2003: The deep-ocean heat uptake in transient climate change. J. Climate, submitted.

[Hughes and Weaver 1994] Hughes T. C. M., and Weaver A. J., Multiple equilibrium of an asymmetric two-basin model, J. Phys. Oceanogr. 24, 619-637 (1994)

[Kamenkovich 2003] I. V. Kamenkovich, A. P. Sokolov, and P. H. Stone, Feedbacks affecting the response of the thermohaline circulation to increasing CO_2: a study with a model of intermediate complexity, Clim. Dyn. DOI 10.1007/s00382-003-0325-5 (2003)

[Keigwin et al. 1994] Keigwin L. D., Curry W. B., Lehman S. J., and Johnsen S., The role of the deep ocean in North Atlantic climate change between 70 and 130 ky ago, Nature 371, 323-327 (1994)

[Keigwin and Boyle 2000] Keigwin, L.D. and E.A. Boyle (2000) Detecting Holocene changes in thermohaline circulation, Proc. Nat. Acad. Sci. 97, 1343-1346 (2000)

[Kitoh et al. 2001] Kitoh A., S. Murakami, and H. Koide, A simulation of the Last Glacial Maximum with a coupled atmosphere/ocean GCM, Geophys. Res. Lett., 28, 2221-2224 (2001)

[Klinger and Marotzke 1999] Klinger B. A., and J. Marotzke, Behavior of double hemisphere thermohaline flow in a single basin, J. Phys. Oceanogr. 29, 382-399 (1999)

[Knutti and Stocker 2002] Knutti, R., and T. F. Stocker, Limited predictability of the future thermohaline circulation close to an instability threshold, J. Climate 15 176-186 (2002)

[Krasovskiy and Stone 1998] Krasovskiy Y. P. and P. H. Stone, Destabilization of the thermohaline circulation by atmospheric transports: An analytic solution, J. Climate 11, 1803-1811 (1998)

[Krinner and Genthon 1998] Krinner, G. and C. Genthon, GCM simulations of the Last Glacial Maximum surface climate of Greenland and Antarctica, Clim. Dyn. 14, 741-758 (1998)

[Latif et al. 2000] Latif M., E. Roeckner, U. Mikolajewicz, and R. Voss, Tropical Stabilization of the Thermohaline Circulation in a Greenhouse Warming Simulation, J. Climate 13, 1809-1813 (2000)

[Levitus 1982] Levitus, S., Climatological atlas of the world ocean, NOAA Professional Paper, vol. 13, U.S. Department of Commerce, NOAA, Washington DC (1982)

[Lucarini and Stone 2003a] Lucarini, V. and P. H. Stone, Thermohaline circulation stability: a box model study - Part I: uncoupled model, submitted to J. Climate. (2003)

[Lucarini and Stone 2003b] Lucarini, V. and P. H. Stone, Thermohaline circulation stability: a box model study - Part II: coupled atmosphere-ocean model, submitted to J. Climate (2003)

[Lucarini and Stone 2003c] Lucarini and Stone, Thermohaline circulation stability: a box model study. Part I: uncoupled model. Part II: coupled atmosphere-ocean

model, Joint Program on the Science and Policy of Global Change Report Series 99 (2003), http://web.mit.edu/globalchange/www/reports.html

[Macdonald and Wunsch 1996] Macdonald A.M., and C. Wunsch, An estimate of global ocean circulation and heat fluxes, Nature 382, 436-439 (1996)

[Manabe and Stouffer 1988] Manabe S., and R. J. Stouffer, Two stable equilibria coupled ocean-atmosphere model, J. Climate 1, 841-866 (1988)

[Manabe and Stouffer 1993] Manabe S., and R. J. Stouffer, Century-scale effects of increased atmospheric CO_2 on the ocean-atmosphere system, Nature 364, 215-218 (1993)

[Manabe and Stouffer 1994] S. Manabe and R. J. Stouffer, Multiple-century response of a coupled ocean/atmosphere model to an increase of atmospheric carbon dioxide, J. Climate, 7, 5-23 (1994)

[Manabe and Stouffer 1999a] Manabe S. and R. J. Stouffer, Are two modes of thermohalince circulation stable?, Tellus, 51A, 400-411 (1999)

[Manabe and Stouffer 1999b] Manabe S. and R. J. Stouffer, The role of thermohaline circulation in climate, Tellus, 51A-B(1), 91-109 (1999)

[Manabe and Stouffer 2000] Manabe, S. and R. J. Stouffer, Study of abrupt climate change by a coupled ocean-atmosphere model, Quaternary Science Reviews, 19 285-299 (2000)

[Marotzke 1996] Marotzke J., Analysis of thermohaline feedbacks, Decadal Climate Variability: Dynamics and predicatibility, Anderson D.L.T. and Willebrand J. Eds., Springer-Verlag, Berlin, pp. 333-378 (1996)

[Marotzke and Willebrand 1991] Marotzke J. and J. Willebrand, Multiple equilibria of the global thermohaline circulation, J. Phys. Oceanogr. 21, 1372-1385.(1991)

[Marotzke and Stone 1995] J. Marotzke and P. H. Stone, Atmospheric transports, the thermohaline circulation, and flux adjustments in a simple coupled model, J. Phys. Ocean., 25, 1350-1364 (1995) .

[Mikolajewicz and Maier-Reimer 1994] Mikolajewicz, U. and E. Maier-Reimer, Mixed boundary conditions in ocean general circulation models and their influence on the stability of the model's conveyor belt, J. Geophys. Res. 99, 22633-22644 (1994)

[Mikolajewicz and Voss 2000] Mikolajewicz U. and R. Voss, The role of the individual air-sea flux components in CO_2-induced changes of the ocean's circulation and climate, Clim. Dyn. 16, 627-642 (2000)

[Nakamura et al. 1994] Nakamura M., P. H. Stone, and J. Marotzke, Destabilization of the thermohaline circulation by atmospheric eddy transports, J. Climate 7, 1870-1882 (1994)

[Peixoto and Oort 1992] Peixoto A. and Oort B., Physics of Climate (American Institute of Physics, 1992)

[Petoukhov et al. 2000] Petoukhov, V., A. Ganopolski, V. Brovkin, M. Claussen, A. Eliseev, C. Kubatzki, and S. Rahmstorf, A climate system model of intermediate complexity. Part I: model description and performance for present climate. Clim. Dyn. 16, 1-17 (2000)

[Rahmstorf 1995] Rahmstorf S., Bifurcations of the Atlantic Thermohaline circulation in response to changes in the hydrological cycle, Nature 378, 145-149 (1995)

[Rahmstorf 1996] Rahmstorf S., On the freshwater forcing and transport of the Atlantic thermohaline circulation, Clim. Dyn. 12, 799-811 (1996)

[Rahmstorf 1997] Rahmstorf S., Risk of sea-change in the Atlantic, Nature, 388, 825-826 (1997)

[Rahmstorf 1999a] Rahmstorf S., Shifting seas in the greenhouse?, Nature, 399, 523-524 (1999)

[Rahmstorf 1999b] Rahmstorf S., Rapid Oscillation of the thermohaline ocean circulation, pp. 139-149 in "Reconstructing ocean history: A window into the future", Abrantes and Mix Eds, (Kluwer Academic/Plenum Publishers, New York, 1999)

[Rahmstorf 1999c] Rahmstorf S., Decadal Variability of the Thermohaline Ocean Circulation, pp. 309-332 in "Beyond El Nio: Decadal and interdecadal climate variability", A. Navarra Ed., (Springer, New York, 1999)

[Rahmstorf 2000] Rahmstorf S., The thermohaline ocean circulation - a system with dangerous thresholds? Climatic Change, 46, 247-256 (2000)

[Rahmstorf 2002] Rahmstorf S., Ocean circulation and climate during the past 120,000 years, Nature 419, 207-214 (2002)

[Rahmstorf 2003] Rahmstorf S., The current climate, Nature 421, 699 (2003)

[Rahmstorf and Willebrand 1995] Rahmstorf S., and Willebrand J., The role of temperature feedback in stabilizing the thermohaline circulation, J. Phys. Oceanogr. 25, 787-805 (1995)

[Rahmstorf and Ganopolski 1999] Rahmstorf S. and A. Ganopolski, Long-term global warming scenarios computed with an efficient coupled climate model, Climatic Change, 43, 353-367 (1999)

[Ramanathan et al. 1979] Ramanathan, V., M. S .Lian, and R. D. Cess, Increased atmospheric CO_2: zonal and seasonal estimates of the effect on the radiation energy balance and surface temperature, J. Geophys. Res., 84, 4949-4958 (1979)

[Roemmich and Wunsch 1985] Roemmich D.H., and Wunsch C., Two transatlantic sections: Meridional circulation and heat flux in the subtropical North Atlantic Ocean, Deep Sea Res., 32, 619-664, (1985)

[Rooth 1982] Rooth C., Hydrology and ocean circulation, Progr. Oceanogr., 11, 131-149 (1982)

[Schmittner and Stocker 1999] Schmittner, A., and T. F. Stocker, The stability of the thermohaline circulation in global warming experiments, J. Climate 12, 1117-1133 (1999)

[Scott et al. 1999] .Scott J. R., J. Marotzke, and P. H. Stone, 1999: Interhemispheric thermohaline circulation in a coupled box model, J. Phys. Oceanogr., 29, 351-365 (1999).

[Seager et al. 2002] R. Seager, D. S. Battistini, J. Yin, N. Gordon, N. Naik, A. C. Clement and M. A. Cane, Is the Gulf Stream responsible for Europe's mild winters?, Q. J. R. Meteorol. Soc. 128, 2563-2586 (2002)

[Shine et al. 1995] Shine, K. P., B. P. Briegleb, A. S. Grossman, D. Hauglustaine, H. Mao, V. Ramaswamy, M. D. Schwarzkopf, R. Van Dorland, and W-C. Wang, Radiative forcing due to changes in ozone: A comparison of different codes, pp 373-396 in "Atmospheric Ozone as a Climate Gas", NATO ASI Series I, Vol. 32 (Springer-Verlag, Heidelberg, 1995)

[Stocker 2000] Stocker T. F., Past and future reorganisations in the climate system. Quat. Sci. Rev. 19, 301-319 (2000)

[Stocker 2001] Stocker T. F., The Role of Simple Models in Understanding Climate Change In: Continuum Mechanics and Applications in Geophysics and the Environment. B. Straugham, R. Greve, H. Ehrentraut, Y. Wang (eds.) Springer Verlag, pp. 337-367 (2001)

[Stocker 2002] Stocker T. F., North-South Connections, Science 297, 1814-1815 (2002)

[Stocker and Wright 1991] Stocker T. F., and D.G. Wright, Rapid transitions of the ocean's deep circulation induced by changes in the surface water fluxes, Nature 351, 729-732 (1991)

[Stocker and Schmittner 1997] Stocker T. F. and A. Schmittner, Influence of CO_2 emission rates on the stability of the thermohaline circulation, Nature, 388, 862-865 (1997)

[Stocker et al. 2001] Stocker, T. F., R. Knutti, G.-K. Plattner, The Future of the Thermohaline Circulation - A Perspective, pp. 277-293 in "The Oceans and Rapid Climate Change: Past, Present, and Future", D. Seidov, M. Maslin, and B. J. Haupt Eds., Volume 126 of Geophysical Monograph (Am. Geophys. Union, Washington D. C., 2001)

[Stommel 1961] Stommel H., Thermohaline convection with two stable regimes of flow, Tellus, 13, 224-230 (1961)

[Stone and Miller 1980] Stone P. H. and D. A. Miller, Empirical relations between seasonal changes in meridional temperature gradients and meridional fluxes of heat, J. Atmos. Sci. 37, 1708-1721 (1980)

[Stone and Yao 1990] Stone P. H. and M. S. Yao, Development of a two-dimensional zonally averaged statistical-dynamical model. Part III: The parametrization of eddy fluxes of heat and moisture. J. Climate 3, 726-740 (1990)

[Stone and Krasovskiy 1999] Stone P. H. and Y. P. Krasovskiy, Stability of the interhemispheric thermohaline circulation in a coupled box model. Dyn. Atmos. Oceans, 29, 415-435 (1999).

[Stouffer et al. 1991] Stouffer, R. J., S. Manabe, and K. Bryan, Climatic response to a gradual increase of atmospheric carbon dioxide, pp. 129-136 in "Greenhouse-Gas-Induced Climatic Change: A Critical Appraisal of Simulations and Observations", (Elsevier Science Publishers, The Netherlands, 1991)

[Stouffer and Manabe 1999] Stouffer, R. J., and S. Manabe, Response of a coupled ocean-atmosphere model to increasing atmospheric carbon dioxide: Sensitivity to the rate of increase. J. Climate 12, 2224-2237 (1999)

[Stouffer and Manabe 2003] Stouffer, R. J., and S. Manabe, Equilibrium response of thermohaline circulation to large changes in atmospheric $CO_2 2$ concentration. Clim. Dyn. 20, 759-773 (2003)

[Titz et al. 2002a] Titz, S., T. Kuhlbrodt, S. Rahmstorf, and U. Feudel, On freshwater-dependent bifurcations in box models of the interhemispheric thermohaline circulation, Tellus A 54, 89-98 (2002)

[Titz et al. 2002b] Titz S. , T. Kuhlbrodt und U. Feudel, Homoclinic bifurcation in an ocean circulation box model, Int. J. Bif. Chaos 12, 869-875 (2002).

[Tziperman 2000a] Tziperman E., Proximity of the Present-Day Thermohaline Circulation to an Instability Threshold, J. of Phys. Ocean. 30, 90-104 (2000)

[Tziperman 2000b] Tziperman E., Uncertainties in thermohaline circulation response to greenhouse warming, Geoph. Res. Lett. 27, 3077-3087 (2000)

[Tziperman et al. 1994] Tziperman E., R. J. Toggweiler, Y. Feliks, and K. Bryan, 1994: Instability of the thermohaline circulation with respect to mixed boundary conditions: Is it really a problem for realistic models? J. Phys. Oceanogr. 24, 217-232 (1994)

[Tziperman and Gildor 2002] Tziperman E. and H. Gildor, The Stabilization of the Thermohaline Circulation by the Temperature/Precipitation Feedback, J. of Phys. Ocean. 32, 2704-2714. (2002)

[Vidal et al. 1999] Vidal L. , R. R. Schneider, O. Marchal, T. Bickert, T. F. Stocker, G. Wefer, Clim. Dyn. 15, 909-919 (1999)

[Wang and Stone 1980] Wang W. C. and P. H. Stone, Effect of ice-albedo feedback on global sensitivity in a one-dimensional radiative-convective climate model, J. Atmos. Sci. 37, 545-552 (1980)

[Wang et al. 1999a] Wang X., Stone P.H., and Marotzke J., Global Thermohaline circulation. Part I: Sensitivity to atmospheric moisture transport, J. Climate 12, 71-82 (1999a)

[Wang et al. 1999b] Wang X., Stone P. H. and J. Marotzke, Global Thermohaline circulation. Part II: Sensitivity with interactive atmospheric transport, J. Climate 12, 83-91 (1999b)

[Weaver and Hughes 1992] Weaver A. J., and T. M. C. Hughes, Stability of the thermohaline circulation and its links to Climate, Trends in Physical Oceanography, Research Trends Series, Council of Scientific Research Integration, Trivandrum, India, 1, 15 (1992)

[Weaver et al. 1999] , Weaver a. J., C.M. Bitz, A. F. Fanning, and M. M. Holland, Thermohaline circulation: high latitude phenomena and the difference between the Pacific and Atlantic, Ann. Rev. Earth Planet. Sci. 27, 231-285 (1999)

[Wiebe and Weaver 1999] Wiebe E. C. and A. J.Weaver, On the sensitivity of global warming experiments to the parametrisation of sub-grid scale ocean mixing. Climate Dyn. 15, 875-893 (1999) .

[Wunsch and Ferrari 2004] Wunsch, C. and R. Ferrari, Vertical Mixing, Energy, and the General Circulation of the Oceans, to appear in Ann. Rev. Flu. Mech. 36, DOI 10.1146 (2004)

[Zhang et al. 1993] Zhang, S., Greatbatch R.J., and Lin C.A., A re-examination of the polar halocline catastrophe and implications for coupled ocean-atmosphere modeling, J. Phys. Oceanogr. 23, 287-289 (1993)